

39. RARE EARTH, MAJOR, AND TRACE ELEMENT COMPOSITION OF LEG 127 SEDIMENTS¹

Richard W. Murray,² Marilyn R. Buchholtz ten Brink,³ Hans-J. Brumsack,⁴ David C. Gerlach,⁵ and G. Price Russ III⁵

ABSTRACT

The relative effects of paleoceanographic and paleogeographic variations, sediment lithology, and diagenetic processes on the final preserved chemistry of Japan Sea sediments are evaluated by investigating the rare earth element (REE), major element, and trace element concentrations in 59 squeeze-cake whole-round and 27 physical-property sample residues from Sites 794, 795, and 797, cored during ODP Leg 127.

The most important variation in sedimentary chemical composition is the increase in SiO₂ concentration through the Pliocene diatomaceous sequences, which dilutes most other major and trace element components by various degrees. This biogenic input is largest at Site 794 (Yamato Basin), moderately developed at Site 797 (Yamato Basin), and of only minor importance at Site 795 (Japan Basin), potentially reflecting basinal contrasts in productivity with the Yamato Basin recording greater biogenic input than the Japan Basin and with the easternmost sequence of Site 794 lying beneath the most productive waters. There are few systematic changes in solid-phase chemistry resulting from the opal-A/opal-CT or opal-CT/quartz silica phase transformations. Most major and trace element concentrations are controlled by the aluminosilicate fraction of the sediment, although the effects of diagenetic silica phases and manganese carbonates are of localized importance.

REE total abundances (Σ REE) in the Japan Sea are strongly dependent upon the paleoceanographic position of a given site with respect to terrigenous and biogenic sources. REE concentrations at Site 794 overall correspond well to aluminosilicate chemical indices and are strongly diluted by SiO₂ within the upper Miocene-Pliocene diatomaceous sequence. Eu/Eu* values at Site 794 reach a maximum through the diatomaceous interval as well, most likely suggesting an association of Eu/Eu* with the siliceous component, or reflecting slight incorporation of a detrital feldspar phase. Σ REE at Site 795 also is affiliated strongly with aluminosilicate phases and yet is diluted only slightly by siliceous input. At Site 797, Σ REE is not as clearly associated with the aluminosilicate fraction, is correlated moderately to siliceous input, and may be sporadically influenced by detrital heavy minerals originating from the nearby rifted continental fragment composing the Yamato Rise.

Ce/Ce* profiles at all three sites increase essentially monotonically with depth and record progressive diagenetic LREE fractionation. The observed Ce/Ce* increases are not responding to changes in the paleoceanographic oxygenation state of the overlying water, as there is no independent evidence to suggest the proper oceanographic conditions. Ce/Ce* correlates slightly better with depth than with age at the two Yamato Basin sites.

The downhole increase in Ce/Ce* at Sites 794 and 797 is a passive response to the diagenetic transfer of LREE (except Ce) from sediment to interstitial water. At Site 795, the overall lack of correlation between Ce/Ce* and La_n/Yb_n suggests that other processes mask the diagenetic behavior of all LREEs. First-order calculations of the Ce budget in Japan Sea waters and sediment indicate that ~20% of the excess Ce adsorbed by settling particles is recycled within the water column and that an additional ~38% is recycled at or near the seafloor. Thus, because the remaining excess Ce is only ~10% of the total Ce, there is not a large source of Ce to the deeply buried sediment, further suggesting that the downhole increase in Ce/Ce* is a passive response to diagenetic behavior of the other LREEs. The REE chemistry of Japan Sea sediment therefore predicts successive downhole addition of LREEs to deeply buried interstitial waters.

INTRODUCTION

The chemical composition of sediments from a marginal ocean basin records the geologic history of the basin and the source terrane(s) from a different perspective than the physical record provided by the sediments themselves. Subtle changes in the redox state of the overlying water, for example, may be recognizable only in the chemical distributions within the sediment column. Variations in the composition of the sedimentary source and in the depositional position of the sediment with respect to metalliferous and terrigenous inputs also affect the chemical composition of sediment. When a sedimentary

grain settles onto the basin floor, however, diagenetic processes begin to modify its chemistry, and the preserved signals of the sedimentary basin's history may change with time. The degree of change will depend on the susceptibility of the element(s) in question to mobilize under diagenetic conditions. In many cases the diagenetic reactions within the sediments provide important information regarding the basin's geologic history.

The sedimentary sequences in the Japan Sea present a terrific opportunity to assess both the chemical sources to fine-grained sediments and the post-depositional diagenetic processes that modify the sediment's primary chemical composition. The Japan Sea is a small, enclosed, marginal ocean basin in which the sedimentary sources and depositional regimes are well characterized by lithostratigraphic sequences recording 2000–5000 m of deposition (Fig. 1). Further resolution of the depositional environments is provided by the wealth of sedimentologic, biostratigraphic, and chemical data collected during Ocean Drilling Program (ODP) Legs 127 and 128. As such, the physical stratigraphic framework is constructed within which chemical variations may be placed. Moreover, Japan Sea sediments are currently undergoing many different stages of diagenesis, including sulfate reduction, silica phase transformations, and carbonate dissolution/recrystallization (Murray et al., this volume), and changes in sediment chemistry may potentially be tied to these diagenetic processes. In particular, the siliceous sequence provides an advantage

¹ Pisciotto, K. A., Ingle, J. C., Jr., von Breyman, M. T., Barron, J., et al., 1992. *Proc. ODP, Sci. Results*, 127/128, Pt. 1: College Station, TX (Ocean Drilling Program).

² Department of Geology and Geophysics, University of California at Berkeley, Berkeley, CA 94720, U.S.A. (Present address: Graduate School of Oceanography, University of Rhode Island, Narragansett, RI 02882, U.S.A.)

³ Earth Sciences Department, Lawrence Livermore National Laboratory, Livermore, CA 94550, U.S.A.

⁴ Geochemisches Institut, Goldschmidtstr. 1, D-3400, Göttingen, Federal Republic of Germany.

⁵ Nuclear Chemistry Division, Lawrence Livermore National Laboratory, Livermore, CA 94550, U.S.A. (Gerlach, present address: Charles Evans and Associates, 301 Chesapeake Drive, Redwood City, CA 94063, U.S.A.; Russ, present address: Chemistry and Material Sciences Department, Lawrence Livermore National Laboratory, Livermore, CA 94550, U.S.A.)

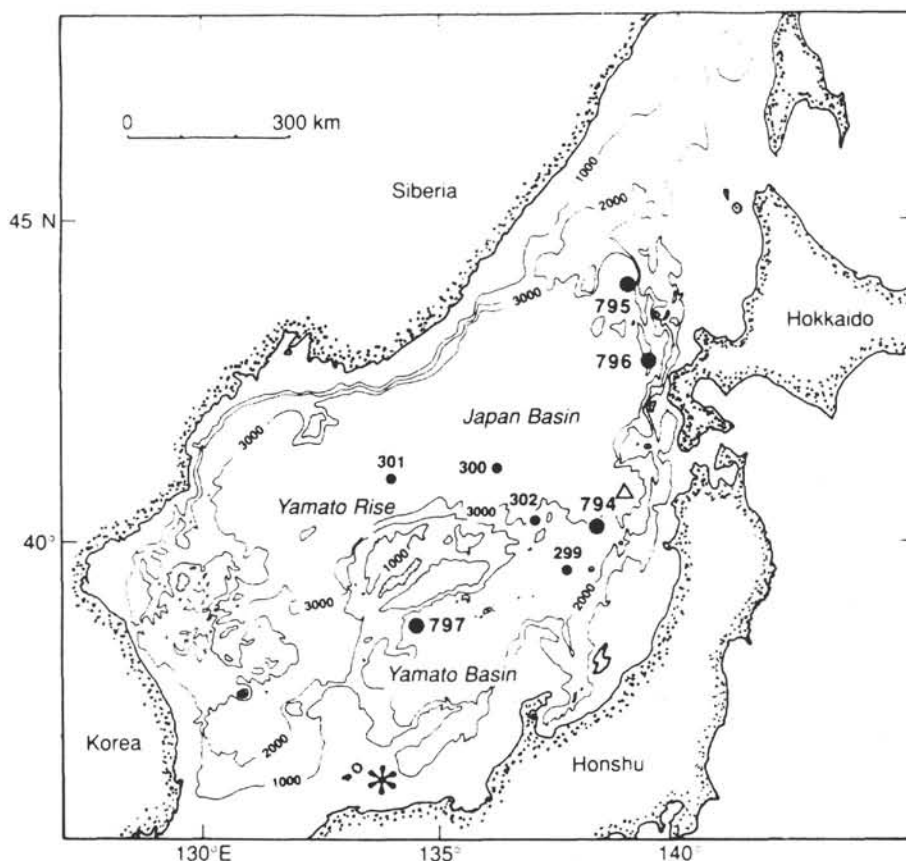


Figure 1. Location map of the Japan Sea showing locations of Leg 127 Sites 794–797 and Deep Sea Drilling Project Leg 31 Sites 299–302. Bathymetry contoured in meters. a marks the approximate position of the study of REEs in settling particles near Site 794 (40.8°N, 138.7°E; Masuzawa and Koyama, 1989); * marks the approximate position of the study of REEs in Japan Sea water (35.7°N, 133.2°E; Tanaka et al., 1990). Map modified from Tamaki, Pisciotto, Allan, et al., 1990.

when addressing large-scale diagenetic changes, as the diagenetic state of the sample can be tracked easily by the SiO_2 phases as they progress through the successive opal-A/opal-CT/quartz diagenetic transitions.

This study attempts to resolve the lithologic and diagenetic parameters that control the chemical composition of Japan Sea sediments. Superimposed on both these effects are paleoceanographic changes that have potentially modified the chemistry of Japan Sea sediments through time. While paleoceanographic variations and paleogeographic location each in turn influence sediment lithology and diagenetic conditions through a given stratigraphic sequence, we restrict our definition of paleoceanographic variations to include those large-scale changes in seawater composition that will substantially influence the rare earth element (REE) record in sediment throughout both Japan Sea basins. By tracking chemical behavior across lithologic, diagenetic, and paleoceanographic boundaries, we address the relative importance of each potential influence under a variety of sedimentologic regimes.

Paleoceanographic Evolution of the Japan Sea

In order to place the chemical variations of the different lithologies of sediments preserved in the Japan and Yamato basins within the proper stratigraphic context, the general paleoceanographic history of the Japan Sea relevant to our chemical investigation is summarized here. Comprehensive presentations of the lithostratigraphic and paleoceanographic changes are presented elsewhere in great detail (Tamaki, Pisciotto, Allan, et al., 1990; plus papers in this volume).

The preliminary paleoceanographic dates and sedimentation rates described herein and used throughout this paper are based on descriptions in Tamaki, Pisciotto, Allan, et al. (1990); more recent values presented in other papers in this volume supersede those used here.

Initial extension and rifting began in the Japan Sea in the early(?) Miocene to early middle Miocene and resulted in the gravity-flow deposition of volcanoclastic sandstones and siltstones along the basin margin. Accelerated deepening of the Yamato Basin during the early Miocene and of the Japan Basin during the early middle Miocene is characterized by fine-grained, diatomaceous and calcareous clay-rich pelagic and hemipelagic muds. Bottom-water (500–1500 m) conditions were most likely oxic to dysaerobic throughout the entire Miocene, as indicated by foraminifer assemblages and bioturbation/lamination character. The three sites (794, 795, and 797) for which chemistry is reported here were either bathymetrically isolated or too distal from terrigenous inputs during this time to receive coarse clastic deposits. Site 797 (Yamato Basin) may have been slightly deeper than Sites 794 and 795. From the late Miocene to the Pliocene, an increase in diatom productivity resulted in hemipelagic diatomaceous and siliceous sedimentation. Bottom waters (1500–2500 m) were generally oxygenated and intrabasin circulation was well developed, although communication between the Yamato and Japan basins may have been restricted during the middle late Miocene. After these highly productive conditions, bathyal hemipelagic muds were deposited from the Pliocene to the present. Sea-level fluctuations may have also affected terrigenous inputs and resulted in periods of anoxic deep water. Within the Quaternary section, preservation of dark-light cycles in silty clays may record fluctuations of terrigenous input, oxy-

genation level, type of organic matter, surface-water productivity, or sedimentation rate. These dark-light cycles are described extensively elsewhere in this volume.

Composite Lithostratigraphic Succession

The lithostratigraphic sequences that result from this paleoceanographic evolution are relatively similar at all three sites studied here (Fig. 2); details of the lithologic successions, terminology usage, and criteria used to divide lithologic units are discussed elsewhere (Tamaki, Pisciotto, Allan, et al., 1990). Silica phase transformations have a profound affect on sedimentary lithology at each site and are located on all chemical profiles. A composite downhole lithostratigraphic sequence is described in the following, with key differences among sites highlighted. Note that the unit numbers do not correlate among the sites (Fig. 2).

The uppermost ~100 m below seafloor (mbsf) consists generally of slightly to highly bioturbated gray clay, silty ashy clay, and diatomaceous clay, which were deposited through the late Pliocene and Quaternary. Discrete ash beds (1–5 cm thick) are a volumetrically minor yet numerous component. Dark-light cycles tend to be more notable in the uppermost tens of meters. Minor calcareous layers (including diagenetic dolomite or ankerite, and manganese carbonates) are found throughout. Diatom abundances decrease toward the base of Unit I at Site 795 and increase toward the base of Unit I at Site 797. Beneath this sequence are moderately to intensely bioturbated diatom and clayey diatom ooze. The age and duration of

deposition of this sequence is different from site to site (Fig. 2). Ash beds (1–5 cm thick) are sparsely disseminated and very rare. Minor dolomitic and dolomitic nodules also occur, usually within concentrations of foraminifers. At Site 794, the lowermost portion of this diatomaceous sequence (Subunit IIB) consists of diatom clay similar to the purer diatom ooze except with less diatoms. Below the diatom ooze is a middle to upper Miocene sequence consisting of moderately to intensely bioturbated diatomaceous clay and faintly laminated siliceous claystone, along with dolomite layers, pyrite, and ash interspersed throughout. Dolomite, ankerite, and silica cements are present locally in small nodules, stringers, lenses and laminae, as are porcelainite and chert layers. The poor recovery through this section at Site 795 may indicate a greater abundance of chert layers than was observed in the recovered samples. Thin carbonate layers are relatively common at Site 797. Beneath the siliceous claystone at Site 794 are moderately bioturbated claystone, silty claystone, and calcareous claystone, with an increasing diagenetic dolomite and ankerite component.

ANALYTICAL METHODOLOGY

Sample Preparation

Most samples in this study are splits of the whole-round squeeze-cake residues from the nylon- and Teflon-lined interstitial-water squeezer described by Brumsack et al. (this volume). The samples were analyzed for their major element, trace element, and REE composition as described in the following. Not every squeeze cake was prepared for geochemical analysis, but the continuity of the

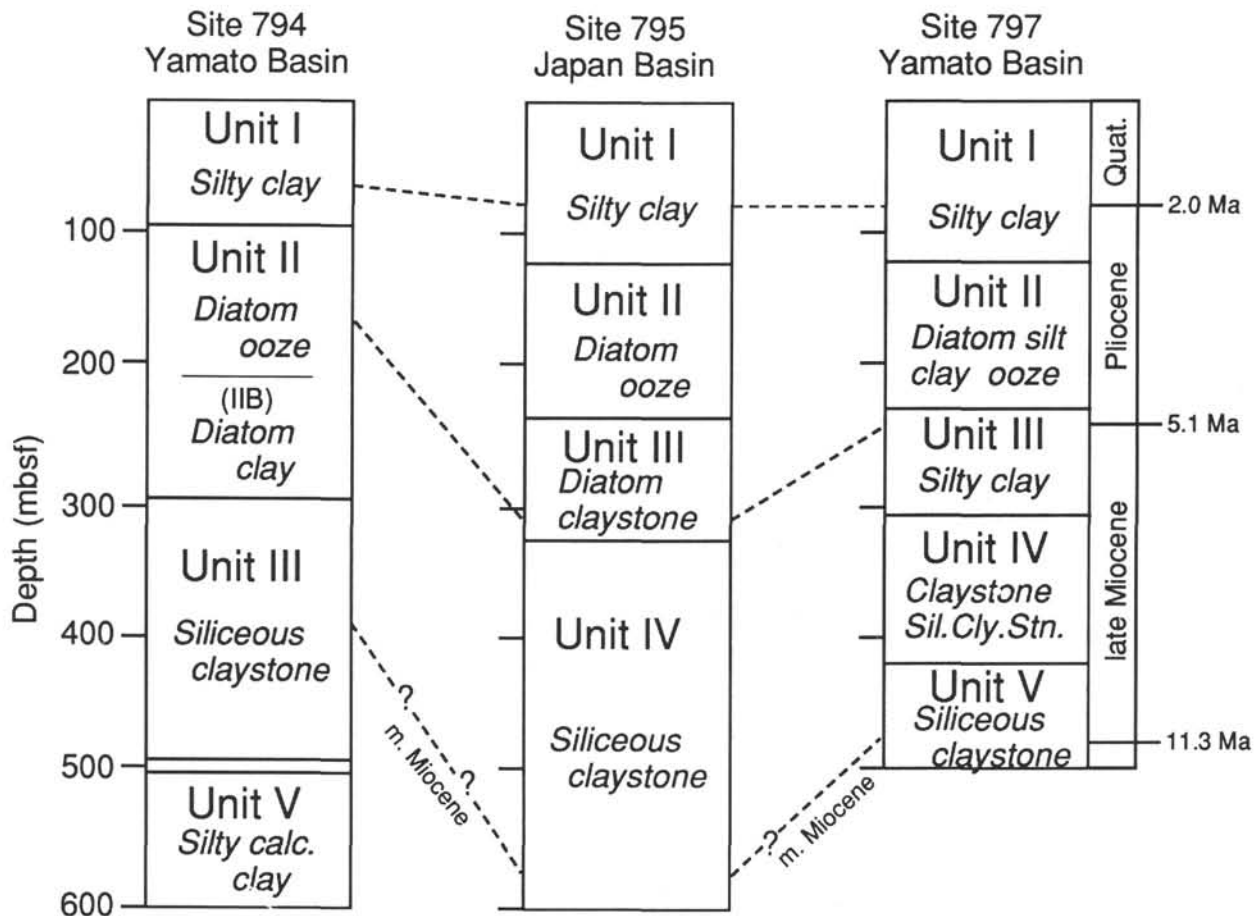


Figure 2. Lithostratigraphic summary of Leg 127 sites analyzed for sedimentary chemistry. Note that the unit numbers do not correlate among the sites. Unit IV at Site 794 was not sampled in this study.

Table 1. Major element data (wt%, volatile free) from Leg 127 squeeze-cake residues and physical-property samples.

Core, section, interval (cm)	Depth (mbsf)	Subunit	SiO ₂	Al ₂ O ₃	CaO	MgO	Na ₂ O	K ₂ O	Fe ₂ O ₃	MnO	TiO ₂	P ₂ O ₅
127-794A-												
1H-3, 140-145	4.4	IA	62.0	17.7	1.01	3.25	3.74	3.53	7.87	0.15	0.71	0.13
3H-5, 140-145	23.7	IA	64.3	17.9	1.71	2.99	2.74	3.62	5.84	0.10	0.70	0.12
6H-4, 145-150	50.8	IA	62.7	15.5	0.71	3.41	2.82	3.33	10.4	0.24	0.76	0.11
9H-4, 145-150	79.3	IB	66.9	16.3	0.71	2.99	2.80	3.52	5.86	0.18	0.69	0.08
12H-4, 145-150	107.8	IIA	70.2	14.0	0.73	2.79	3.01	2.90	5.39	0.37	0.58	0.08
15H-4, 145-150	136.3	IIA	79.2	9.29	0.45	2.04	2.60	2.02	3.77	0.17	0.39	0.06
22X-4, 145-150	203.5	IIA	80.8	8.60	0.48	2.20	2.17	1.70	3.42	0.21	0.35	0.05
25X-4, 145-150	232.5	IIIB	71.6	11.0	1.11	4.14	2.49	2.24	5.09	1.83	0.44	0.07
29X-4, 145-150	271.4	IIIB	65.3	15.2	0.68	4.74	3.06	3.07	6.79	0.49	0.61	0.08
33X-2, 140-145	309.2	IIIA	67.3	15.0	0.63	4.13	2.14	3.42	6.30	0.39	0.61	0.10
36X-4, 145-150	337.9	IIIA	66.5	15.3	0.67	4.52	2.50	3.41	5.71	0.72	0.58	0.07
127-794B-												
12R-1, 145-150	406.4	IIIB	79.9	9.16	2.17	1.98	1.41	1.72	3.18	0.08	0.36	0.06
18R-4, 145-150	468.5	IIIB	74.3	11.1	0.43	4.76	1.45	2.98	4.33	0.13	0.42	0.08
24R-2, 140-145	523.7	V	64.3	12.6	2.42	4.88	1.61	4.19	6.62	2.75	0.48	0.15
127-795A-												
1H-4, 145-150	6.0	IA	64.1	17.2	1.27	3.07	2.79	3.36	7.03	0.39	0.73	0.14
2H-4, 145-150	15.3	IA	64.5	17.2	1.08	3.15	2.54	3.56	6.92	0.15	0.75	0.13
3H-4, 145-150	24.8	IA	64.6	15.1	1.08	3.37	2.95	3.10	8.58	0.51	0.59	0.11
4H-4, 145-150	34.8	IA	62.3	17.0	1.20	3.01	2.64	3.21	9.62	0.21	0.71	0.14
5H-4, 145-150	43.8	IA	66.1	15.8	1.50	2.35	3.68	3.41	6.37	0.18	0.59	0.10
6H-4, 145-150	53.8	IA	66.9	15.3	1.15	2.85	3.02	2.99	7.00	0.12	0.63	0.12
7H-4, 145-150	62.8	IA	65.8	17.0	1.01	3.09	3.12	3.27	5.71	0.24	0.72	0.11
8H-4, 145-150	72.3	IA	63.3	16.9	1.06	3.07	2.98	3.22	7.85	0.73	0.73	0.11
9H-4, 145-150	81.8	IA	64.5	16.4	0.86	3.15	2.99	3.30	7.85	0.17	0.71	0.10
10H-1, 145-150	86.8	IB	65.4	17.2	0.93	3.05	2.82	3.42	6.09	0.11	0.75	0.12
12H-4, 140-145	110.2	IB	67.7	14.6	1.16	2.97	2.87	2.81	7.00	0.24	0.61	0.10
15H-4, 140-145	138.7	II	70.9	13.2	0.83	2.88	2.48	2.52	6.45	0.09	0.55	0.08
18H-4, 140-145	158.8	II	71.4	13.3	1.06	2.51	2.62	2.48	5.84	0.10	0.55	0.08
21X-4, 140-145	187.5	II	77.3	10.8	0.72	2.02	2.40	2.07	4.11	0.09	0.47	0.07
25X-3, 140-145	224.8	II	71.4	13.1	0.89	2.83	2.57	2.53	5.87	0.16	0.58	0.08
29X-2, 140-145	262.4	IIIA	74.6	11.8	1.09	2.35	2.58	2.08	4.84	0.09	0.52	0.07
30X-2, 145-150	272.3	IIIA	73.3	11.9	0.93	2.48	2.55	2.23	5.79	0.10	0.62	0.09
31X-4, 145-150	285.1	IIIA	75.2	11.3	0.98	2.12	2.49	2.07	5.12	0.09	0.57	0.08
^a 34X-1, 100-102	308.9	IIIB	73.9	11.1	0.95	2.22	3.82	2.20	5.13	0.09	0.55	0.08
^a 34X-3, 100-102	311.9	IIIB	72.4	12.2	1.00	2.58	3.27	2.29	5.36	0.09	0.63	0.09
^a 34X-4, 100-102	313.4	IIIB	75.5	11.7	0.98	2.61	2.51	2.00	4.03	0.08	0.53	0.07
34X-5, 140-145	315.3	IIIB	74.0	12.3	0.88	2.39	2.75	2.27	4.75	0.08	0.57	0.08
^a 34X-6, 100-102	316.4	IIIB	75.3	12.1	0.84	2.80	2.41	1.95	3.90	0.08	0.56	0.06
^a 34X-7, 39-40	317.3	IIIB	74.7	11.6	1.10	1.84	3.46	2.42	4.25	0.08	0.50	0.08
^a 35X-1, 100-102	318.6	IIIB	74.8	11.0	0.81	2.30	3.46	2.18	4.77	0.08	0.54	0.07
35X-2, 145-150	320.6	IIIB	76.3	11.3	0.72	2.17	2.36	1.93	4.58	0.08	0.54	0.08
^a 35X-3, 100-102	321.6	IIIB	77.0	10.3	0.86	2.01	2.95	1.91	4.29	0.07	0.51	0.08
^a 35X-4, 100-102	323.1	IIIB	73.4	12.1	0.96	2.44	2.89	2.19	5.26	0.08	0.61	0.09
^a 35X-6, 100-102	326.1	IIIB	70.2	13.5	0.98	2.70	3.04	2.50	6.15	0.08	0.69	0.09
^a 37X-1, 99-100	337.9	IVA	80.5	9.1	0.62	1.68	2.14	1.69	3.73	0.05	0.46	0.07
37X-1, 145-150	338.4	IVA	76.9	10.8	0.66	2.02	2.37	2.02	4.51	0.07	0.51	0.07

profiles was assured. Samples were split aboard *JOIDES Resolution* by cutting with a knife down the longitudinal axis of the compressed cake. An additional suite of physical-property residue samples from Sites 795 and 797 were split aboard the ship and analyzed for major and trace elements (no REE) as described in the following. On shore, after oven-drying at ~150°C for 3–5 hr, all samples were powdered by hand in an agate mortar and pestle.

Analytical Procedure and Uncertainty

Approximately 20 g of squeeze-cake residue was powdered and split for REE and major/trace element analysis. Major and trace elements were analyzed by X-ray fluorescence (XRF) at X-Ray Assay Laboratories, Don Mills, Ontario, Canada. REEs were analyzed by ICP-mass spectrometry (ICP-MS) at Lawrence Livermore National Laboratory. Complete sample dissolution prior to introduction into the ICP-MS was achieved by HNO₃-HF-HClO₄ microwave digestion

in sealed Teflon beakers, as detailed elsewhere (Murray et al., 1991). Samples were prepared and run in random order (i.e., mixed sites and depths) on different analytical runs, days, and ICP-MS instruments. Values of Ba determined from XRF were used to correct for ionization suppression of REEs (average ~30%) during ICP-MS analysis; the accuracy for REEs therefore is as good as the Ba XRF values (5%–≤10%). Replicate analyses of solutions indicate that the precision of the Ba ionization correction is ±4% for light REEs (LREEs; La to Nd) and ±8% for heavy REEs (HREEs; Er to Lu), even though the % suppression is nonreproducible and may vary between runs of the same solution on different days by 10%–20%. As determined by replicate analyses of USGS reference rocks MAG-1, SCO-1, and SGR-1 (Taylor and McLennan, 1985; Jarvis and Jarvis, 1985), the general precision of the ICP-MS analysis is ~≤5% for LREEs and 5%–10% for HREEs (Murray et al., 1991). Gd is systematically higher (18%) in the reference rocks, which is most likely due to interferences on ¹⁵⁷Gd from ¹³⁸BaF⁺ or ¹⁴⁰CeOH⁺⁺ (Murray et al.,

Table 1 (continued).

Core, section, interval (cm)	Depth (mbsf)	Subunit	SiO ₂	Al ₂ O ₃	CaO	MgO	Na ₂ O	K ₂ O	Fe ₂ O ₃	MnO	TiO ₂	P ₂ O ₅
127-795B-												
1R-1, 140-145	366.6	IVA	67.3	15.2	0.84	2.67	2.38	2.97	7.84	0.08	0.68	0.10
^a 9R-2, 111-113	445.0	IVB	88.1	5.7	0.38	0.90	1.17	1.15	2.26	0.03	0.27	0.04
^a 11R-3, 81-83	464.0	IVB	72.5	13.8	0.84	2.27	1.96	2.56	5.28	0.08	0.58	0.07
^a 12R-3, 96-98	475.4	IVB	73.4	13.5	0.76	2.15	1.82	2.64	5.03	0.08	0.57	0.07
13R-2, 140-145	483.9	IVB	70.9	14.5	0.96	2.21	1.97	2.73	6.08	0.07	0.64	0.07
^a 13R-3, 63-65	484.6	IVB	72.2	14.1	0.70	2.16	1.95	2.71	5.39	0.07	0.58	0.06
^a 14R-3, 127-129	495.0	IVB	63.4	19.0	2.07	2.36	2.31	1.81	8.21	0.06	0.63	0.14
19R-1, 140-145	540.1	IVB	79.0	11.2	0.64	1.58	1.33	2.11	3.69	0.03	0.46	0.05
127-796A-												
2H-4, 145-150	9.2	IA	65.3	17.2	1.89	2.75	3.00	2.87	6.09	0.09	0.70	0.14
5H-5, 145-150	39.2	IA	62.1	15.6	6.62	2.47	2.64	2.95	6.81	0.11	0.64	0.13
9X-2, 145-150	61.8	IB	67.1	16.0	1.61	2.54	2.80	2.90	6.20	0.17	0.67	0.10
11X-1, 145-150	79.8	IB	67.6	15.9	1.74	2.55	2.97	2.68	5.66	0.10	0.70	0.10
127-797B-												
1H-2, 145-150	3.0	IA	62.6	17.3	1.19	3.28	2.65	3.68	8.30	0.09	0.74	0.15
2H-4, 145-150	11.9	IA	60.5	17.3	1.31	2.93	2.74	3.43	10.8	0.11	0.77	0.16
3H-5, 140-145	22.8	IA	65.0	18.0	0.76	3.13	2.37	3.78	5.85	0.09	0.83	0.14
4H-4, 145-150	30.9	IA	57.6	16.4	9.62	3.30	2.20	3.29	6.47	0.33	0.71	0.13
5H-4, 145-150	40.4	IA	62.5	17.8	1.01	3.06	3.00	3.71	7.81	0.35	0.71	0.12
6H-4, 140-145	49.8	IA	65.1	17.7	0.71	2.87	2.74	3.45	6.41	0.28	0.66	0.10
7H-4, 145-150	59.4	IA	65.0	17.4	0.81	3.25	2.51	3.66	6.33	0.23	0.70	0.11
8H-4, 145-150	68.9	IA	67.4	16.1	0.74	2.82	2.59	3.17	6.12	0.30	0.64	0.09
9H-4, 140-145	78.3	IA	64.9	17.8	0.96	2.08	3.71	4.14	5.48	0.15	0.66	0.12
10H-4, 145-150	87.9	IB	66.6	16.0	0.60	3.27	2.47	3.36	6.67	0.18	0.72	0.09
12H-4, 145-150	106.9	IB	66.9	15.9	1.03	1.93	3.88	4.02	4.98	0.88	0.52	0.09
15H-4, 145-150	135.4	II	64.1	17.2	0.58	3.64	2.68	3.37	7.21	0.43	0.69	0.09
18H-4, 145-150	163.9	II	59.8	9.93	5.47	3.30	1.70	2.05	4.28	12.9	0.37	0.17
21X-4, 140-145	191.4	II	75.1	12.1	0.39	2.71	2.05	2.39	4.56	0.20	0.52	0.07
24X-5, 140-145	221.7	II	75.3	11.1	0.43	2.75	2.05	2.19	5.27	0.28	0.52	0.08
27X-6, 140-145	252.3	III	69.3	14.4	0.57	3.53	2.51	2.62	6.03	0.26	0.59	0.08
28X-1, 145-150	254.6	III	67.1	14.6	0.68	4.37	2.54	2.74	6.81	0.35	0.70	0.10
^a 30X-1, 99-101	273.5	III	63.2	15.7	0.91	4.43	4.23	2.96	7.38	0.29	0.74	0.12
30X-1, 145-150	274.0	III	68.6	14.5	1.04	3.65	2.40	2.59	6.20	0.25	0.65	0.14
^a 31X-2, 98-100	284.7	III	69.1	13.0	1.01	3.38	4.02	2.28	6.39	0.21	0.58	0.13
^a 31X-5, 96-98	289.2	III	64.2	15.4	1.17	4.48	3.47	3.00	6.82	0.55	0.76	0.14
^a 32X-2, 98-100	294.4	III	65.0	15.1	1.25	4.06	3.87	2.63	6.85	0.26	0.72	0.20
32X-3, 145-150	296.4	III	65.8	16.2	0.94	4.10	2.65	2.86	6.44	0.24	0.69	0.14
^a 32X-5, 99-100	298.9	III	65.2	15.4	0.81	4.19	3.17	2.93	7.16	0.23	0.71	0.12
^a 33X-1, 100-101	302.5	IVA	63.8	15.8	0.89	4.58	3.09	3.05	7.55	0.31	0.75	0.11
33X-2, 145-150	304.5	IVA	64.1	16.7	0.69	4.36	2.72	3.29	7.04	0.32	0.70	0.10
^a 33X-3, 100-101	305.5	IVA	63.6	16.7	0.97	3.82	3.05	3.39	7.37	0.24	0.74	0.14
34X-2, 145-150	314.2	IVA	62.9	17.5	0.94	3.87	2.48	3.93	6.83	0.81	0.72	0.13
^a 42X-1, 47-49	388.4	IVB	82.9	7.3	0.36	2.08	1.50	1.56	3.78	0.11	0.32	0.08
^a 44X-1, 29-31	407.6	IVB	88.4	5.2	0.34	1.75	1.24	1.06	1.58	0.06	0.24	0.06
^a 46X-1, 40-42	427.0	V	84.5	6.9	0.42	1.93	1.56	1.54	2.73	0.08	0.31	0.08
^a 47X-1, 107-109	437.3	V	75.3	11.8	0.52	3.39	1.74	2.62	3.94	0.12	0.45	0.08
^a 48X-1, 100-102	446.9	V	81.9	7.5	0.45	3.61	1.43	1.72	2.96	0.13	0.31	0.07

Note: Analyses by XRF at X-Ray Assay Laboratories, Don Mills, Ontario, Canada.

^a Physical-property residue sample.

1991), although visual inspection of shale-normalized plots of data from this study do not show a systematic Gd enrichment. Final LREE concentrations agree well ($\pm 4\%$) with previous studies of other Japan Sea sediments determined by instrumental neutron activation analysis (Masuzawa and Koyama, 1989); HREE data are difficult to compare as a result of the non-shale-like Tb, Yb, and Lu ratios presented in the data table of Masuzawa and Koyama (1989), as well as the lack of HREE agreement between their table and shale-normalized REE plot.

REE Terminology

REE abundances in marine sediments commonly are normalized to average shale values to minimize the effect of the odd-even variability in elemental abundances. Normalization values used here (Table 1) are an average of North American, European, and Russian

shale composites used by previous workers; note that Tb values from this composite are probably too high, causing an apparent Tb depletion in the shale-normalized REE plot (Murray et al., 1991). Tm and Lu values may also be high (R. L. Korotev, pers. comm., 1991). Nevertheless, we use these values because they are widely used by marine chemists (see discussion in Sholkovitz, 1988) and are therefore of most use for comparing results between studies of ocean waters and marine sediment. Moreover, use of the North American Shale Composite (NASC) for ICP-MS REE data is handicapped because not all HREEs in NASC are analyzed by a common technique (Gromet et al., 1984). Shale values used here for normalization purposes do not necessarily represent the average REE terrigenous input pattern (Sholkovitz, 1988, 1990; Condie, 1991). We calculate the Ce anomaly using the ratio $Ce/Ce^* = (Ce_{\text{sample}}/Ce_{\text{shale}})/Ce^*$, where Ce^* is the predicted value obtained by linear interpolation between

shale-normalized La and Pr values. The Eu anomaly (Eu/Eu^*) is calculated similarly, using values of shale-normalized Sm and Gd. Ce/Ce^* and/or $\text{Eu}/\text{Eu}^* \sim 1$ does not imply flatness across any portion of the shale-normalized REE spectrum, including the Ce and Eu regions. Precision of Ce/Ce^* and Eu/Eu^* is estimated to be $\sim 5\%$, with accuracy estimated at $\leq 10\%$ for Ce/Ce^* and higher for Eu/Eu^* because of potential interferences on Gd ($\leq 15\%$, see previous discussion). Contrasts in LREE vs. HREE behavior are quantified by the ratio $\text{La}_n/\text{Yb}_n = (\text{La}_{\text{sample}}/\text{La}_{\text{shale}})/(\text{Yb}_{\text{sample}}/\text{Yb}_{\text{shale}})$.

RESULTS AND DISCUSSION

Major element (volatile free), REE, and trace element data for all Leg 127 sites are reported in Tables 1 and 2, and the respective concentration profiles are also presented for Sites 794, 795, and 797 (Figs. 3 through 5). Concentration data from Site 796 are presented in Tables 1 and 2 but are not discussed, as only four samples were analyzed. Correlation coefficient values (r) between various elements at each site are listed in Tables 3 through 5; except where noted, listed values are for correlations through the entire sequence and may mask local associations not visible at discrete intervals. Throughout the discussion, we often reference data to Al because it is primarily from a terrigenous source and can therefore be used to monitor varying terrestrial inputs and because Al is relatively insoluble and immobile during diagenesis (e.g., Hower et al., 1976; Boles and Franks, 1979). Results are presented here on a site-by-site basis in order to synthesize the different styles of chemical behavior responding to the lithologic and diagenetic influences through a common stratigraphy. Site 794 is discussed in the greatest detail, as many of the aspects of chemical behavior at Site 794 are observed at Sites 795 and 797 and need not be repeated. The site presentations are followed by discussion of the REE compositions of Japan Sea sediments and their implications for the sedimentary history of the Japan Sea.

The downhole profiles of the raw concentration data allow assessment of the broad associations of particular elements to different lithologies. For example, as will be shown in the following, SiO_2 concentrations are commonly associated with diatomaceous sequences. The Al-normalized profiles show how an element's concentration changes with respect to terrigenous input. If a given Al-normalized profile records elemental behavior that cannot be related to the inferred terrigenous or siliceous inputs, then the element must be responding to a third parameter, for example, phosphate. In all profiles, significant deviations ($\pm 15\%$) from the average, especially if part of a larger trend, may be interpretable in the context of stratigraphic heterogeneity controlled by local parameters. In some cases, comparison between different profiles on a point-by-point basis elucidates the causes behind the perturbations. In other cases, however, sharp and isolated increases or decreases in concentration are not associated between elements at the same site, which limits successful interpretation.

Site 794

Major Elements

The most important variation in major element concentrations at Site 794 is the varying SiO_2 concentration, which dilutes concentrations of the other major elements to different degrees (Fig. 3A and Table 3). This is seen clearly, for example, through the diatom ooze and diatomaceous clay of Unit II, where SiO_2 concentrations reach a maximum of 80.8 wt% in Subunit IIA, before decreasing through the siliceous clays of Subunit IIB. SiO_2 concentrations remain essentially constant at ~ 66 wt% through the opal-A/opal-CT diagenetic transition. The elevated SiO_2 values below the opal-CT/quartz transition within Subunit IIIB may reflect the increasing amount of silica cements, stringers, and lenses in Subunit IIIB (Tamaki, Pisciotto, Allan, et al., 1990). Within the claystones of Unit V, SiO_2 concentrations return to average shale values.

In addition to the expected Si/Al increase, the Na/Al ratio also increases through Unit II (Fig. 3B). This profile may reflect a strong affiliation of Na with the biogenic opal or an affiliated clay phase, with Na being adsorbed from either interstitial waters or seawater, as suggested by Donnelly and Merrill (1977), or perhaps may record an inherited chemical signature from detrital inputs (e.g., plagioclase feldspar) that are not uniform through time. We will discuss these and other potential causes further, in the context of the Eu/Eu^* data.

Other Al-normalized major element profiles show downhole variation at Site 794 (Fig. 3B). K/Al, Fe/Al, Mn/Al, Ca/Al (excepting one point), Mg/Al, and P/Al increase from Unit III to Unit V, the same interval through which Si/Al decreases, implying response to the concentration of the siliceous component. Alternatively, these increases may reflect the diagenetic formation of carbonate/phosphate within and below Unit III. Fe/Al also shows a relative maximum within the diatom clay of Subunit IIB. The overall slight Mg/Al increase from the seafloor through the diatomaceous ooze of Subunit IIA is consistent with an additional Mg component potentially recording adsorption onto biogenic opal (e.g., Donnelly and Merrill, 1977).

Rare Earth Elements

The REEs are affected by increases and decreases in the biogenic SiO_2 component at Site 794, as shown by $r = -0.93$ between ΣREE and SiO_2 (Table 6) and visually apparent from the pronounced ΣREE minima through the siliceous Subunit IIA and ΣREE increases from Unit III to Unit V (Fig. 4 and Table 2). $\Sigma\text{REE}/\text{Al}$ values are essentially constant through Unit II, indicating an association of REEs with aluminosilicate phases. This is also suggested by high r values between ΣREE and Al_2O_3 , TiO_2 , K_2O , Fe_2O_3 , and P_2O_5 , which tend to be present in shale-like relative abundances (e.g., Gromet et al., 1984). As such, all may be responding to the SiO_2 dilution.

Ce/Ce^* values are all positive and increase consistently from values of ~ 1.08 for shallow samples to a maximum of $\text{Ce}/\text{Ce}^* = 1.61$ within the siliceous claystone of Subunit IIIA (Fig. 4). The near-surface values are consistent with the Ce/Ce^* value ~ 1.07 reported by Masuzawa and Koyama (1989) from surficial sediment 50–100 km north of Site 794 (Fig. 1). There is no change in trend through the diatomaceous interval of Unit II, nor is there a change in value across the opal-A/opal-CT diagenetic transition. Ce/Ce^* decreases sharply to $\text{Ce}/\text{Ce}^* = 1.15$, however, across the opal-CT/quartz transition between Subunits IIIA and IIIB. As discussed previously, SiO_2 concentrations tend to increase through this interval as well, which suggests that the Ce/Ce^* decrease is a diagenetic change, with the newly precipitating biogenic quartz phases recording a lower Ce/Ce^* value than the primary sediment. The relatively high r value between Ce/Ce^* and MnO (0.81; Table 6) suggests that the excess Ce is associated with Mn.

Eu/Eu^* varies only slightly through the sedimentary column, averaging 1.03 ± 0.05 , except for a large and systematic increase within the diatom ooze of Unit II, where Eu/Eu^* peaks at 1.28 (Fig. 4). The correlation coefficient of $r = 0.69$ between Eu/Eu^* and SiO_2 suggests that Eu/Eu^* is affiliated with the biogenic siliceous component, which is controlling the negative r values between Eu/Eu^* and the remaining elements (Table 6). There is essentially no change in Eu/Eu^* across either the opal-A/opal-CT or opal-CT/quartz diagenetic boundary. The single high Eu/Eu^* point in Unit III corresponds with large decreases in CaO and Sr and with an increase in La_n/Yb_n ; no other major or trace elements deviate significantly in that sample from the overall trend.

Shale-normalized Eu anomalies have been reported only from marine waters affected by aeolian input ($\text{Eu}/\text{Eu}^* < 1$) or hydrothermal input ($\text{Eu}/\text{Eu}^* > 1$; Elderfield, 1988). Neither of these potential inputs can be responsible for the observed positive Eu anomalies through the diatomaceous Unit II sequence as (1) the Eu anomaly peak at Site 794 is positive, not negative, and (2) there clearly is no independent

evidence of hydrothermal input into the sequences (e.g., metalliferous sediment or $Ce/Ce^* \ll 1$, and Fe_2O_3 averages a low 5.75 ± 1.90). Eu/Eu^* is not likely to respond to diagenetic influences within the sediment column (see discussion in McLennan, 1989). The relationship between Eu/Eu^* and SiO_2 implies that the siliceous component is carrying a slightly positive Eu anomaly, although this would require Eu fractionation during construction of diatom tests or during adsorption from seawater and/or incorporation of a Eu-enriched phase into or onto diatom tests. A slight relative increase in the primary detrital feldspar component could also cause an inherited positive Eu/Eu^* anomaly in the bulk sediment, even if the feldspars have been diagenetically altered, due to the high Eu/Eu^* of plagioclase and alkali feldspars (e.g., $Eu/Eu^* \sim 7\text{--}40$; Dymek and Gromet, 1984; Taylor and McLennan, 1985). The coincidence of the peaks in Eu/Eu^* and Na/Al may also be consistent with the presence of a detrital feldspar component in this interval, although the small feldspar component implied by the slight bulk Eu/Eu^* increase (from ~ 1 to ~ 1.3) relative to feldspar Eu/Eu^* ($\sim 7\text{--}40$, as noted previously) may not supply sufficient Na to generate the Na/Al increase. Although the fact that the Eu enrichment occurs only at Site 794 (where the biogenic input is most pronounced) argues for a siliceous influence, we cannot rigorously resolve these potential mechanisms given the current data base, and we hope that additional information about this interval will be gained from mineralogical studies at this site (e.g., Fagel et al., 1991).

La_n/Yb_n values, which indicate the relative behavior of LREEs to HREEs, remain in the range ~ 0.97 to ~ 1.34 through Units I and II (Fig. 4), only slightly less than the estimated average terrigenous input of La_n/Yb_n of ~ 1.3 suggested by Sholkovitz (1990) and generally agreeing with the value of ~ 1 suggested by Condie (1991). Within the diatomaceous ooze of Subunit IIA, La_n/Yb_n values reach a relative minimum of 0.97 and increase through the diatomaceous clay of Subunit IIB to $La_n/Yb_n = 1.34$. Below Unit II, La_n/Yb_n values show more scatter, yet on average are lower in the siliceous claystones of Unit III and the silty calcareous clay of Unit V. The low La_n/Yb_n value of 0.69 is coincident with high CaO and Ca/Al. The potential for a causal link between the changes in La_n/Yb_n and Ce/Ce^* below the opal-A/opal-CT transition at Site 794 will be addressed later.

Trace Elements

Cr, Rb, Y, Zr, and Nb concentrations all have similar downhole profiles that decrease through Subunit IIA (Fig. 5A); concentrations also correlate negatively with the SiO_2 concentration (Table 3) indicating that these elements are not associated with the biogenic sedimentary component. Ba is enriched slightly through Subunit IIA, although Sr values are within the same range as Sr values in the silty clays and siliceous claystones above and below the interval.

The essentially constant Al-normalized profiles of Rb, Zr, and Nb (Fig. 5B) further suggest that these elements are affiliated predominantly with the aluminosilicate phase. Most r values of the trace elements are greatest with Al_2O_3 and TiO_2 (Table 3). Of these elements, however, Y/Al is enriched in the clay-rich diatomaceous Subunit IIB, and Nb/Al seems slightly elevated through the siliceous claystone of Unit III. Cr/Al may be slightly higher through the diatomaceous interval of Unit II and also through portions of the siliceous claystones of Unit III, implying that a portion of the Cr is carried by the siliceous component. Sr/Al and Ba/Al clearly are enriched through the diatomaceous intervals, confirming their biogenic associations.

Site 795

Major Elements

The diatom-rich sequences at Site 795 (Units II and III), although relatively high in SiO_2 , do not show the well-developed SiO_2 maximum that is present at Site 794 (Fig. 3A). Instead, SiO_2 concentrations gradually increase from near-surface values of ~ 64 wt% to a maxi-

um of ~ 77 wt% at the opal-A/opal-CT transition (~ 325 mbsf). These maximum concentrations are slightly lower than the maximum SiO_2 observed at Site 794 (~ 81 wt%). The SiO_2 scatter through Unit IV is affected by sampling resolution and reflects the increasing abundance of diagenetic porcellanite and chert sequences, which commonly contain zones of elevated SiO_2 concentrations. The remaining major elements show absolute concentrations that generally follow Al and are diluted by the SiO_2 component (Fig. 3A and Table 4).

Si/Al also shows a only slight increase through the ooze (Fig. 3B), consistent with the minimal SiO_2 increase described previously. Below the opal-A/opal-CT transition, Ti/Al, Na/Al, Fe/Al, and Mg/Al all decrease to minimum values at depth (Fig. 3B), implying some diagenetic behavior, although the specific relationships are unclear. The Na/Al profile does not show the pronounced maximum through the siliceous interval that was recorded at Site 794 (Unit II at both sites). Al-normalized Ca, P, and, most noticeably, Fe profiles each show an increase from the diatom ooze of Unit II to a relative maximum through the diatom claystones of Unit III (Fig. 3B).

Rare Earth Elements

Σ REE concentrations at Site 795 decrease from ~ 190 to ~ 160 ppm through Unit I, decrease further to ~ 115 ppm in the diatom ooze of Unit II, and decrease only slightly to the base of Unit III, where Σ REE is ~ 100 ppm (Fig. 4). Σ REE appears higher in the siliceous claystones of Unit IV, although only a few samples were analyzed. The high Σ REE and Σ REE/Al at 43.7 mbsf are coincident with an anomalously low Eu/Eu^* as well as high Na_2O and Zr concentrations. Interelement correlations (Table 6) show that the REEs are only slightly diluted by the siliceous biogenic component and are closely affiliated with the aluminosilicate component (Al_2O_3 , $r = 0.92$; K_2O , $r = 0.94$). The other high r values (e.g., P_2O_5) also reflect the aluminosilicate input, as the Al-normalized major element ratios are similar to that of average shale, as at Site 794.

The Ce/Ce^* profile increases from values ranging between 0.98 and 1.11 in Unit I to higher values (~ 1.30) at depth in Unit IV (Fig. 4). There is no change in Ce/Ce^* across either the opal-A/opal-CT or opal-CT/quartz diagenetic transition. Correlation coefficients, however, suggest a weak and negative association with virtually all components except SiO_2 , most likely reflecting a SiO_2 dilution effect (Table 6). Note, however, that unlike at Site 794 Ce/Ce^* does not correlate with MnO. Most Eu/Eu^* values range between 0.90 and 1.08 and are essentially uniform (within error; Fig. 4). The anomalously low Eu/Eu^* in Unit I corresponds with high Σ REE, as described previously. Unlike at Site 794, there is no Eu/Eu^* maximum within the diatom ooze of Unit II (nor is there a concomitant Na or Na/Al increase).

The La_n/Yb_n profile (Fig. 4) can be divided into three sections: (1) increasing from ~ 1 to ~ 1.25 through Unit I claystones, (2) decreasing to a broad relative minimum of ~ 0.84 through the diatom ooze of Unit II and diatomaceous claystone of Unit III, and (3) increasing again to 1.26 through Unit IV siliceous claystones. Despite the continuity of the profile, La_n/Yb_n correlates only moderately (and negatively) with SiO_2 and Eu/Eu^* (Table 6). The low La_n/Yb_n ($= 0.49$) at the base of Unit I is coincident with high Eu/Eu^* and low Ce/Ce^* , as well as high Mn/Al and Ca/Al, and as such probably reflects REE fractionation within a manganese carbonate.

Trace Elements

Some trace element profiles at Site 795 (Fig. 5A) are generally smooth through the entire sequence (e.g., Sr, Zr), although others show scatter around a constant trend (e.g., Nb). Chromium concentrations double within Unit III to values between 120 and 160 ppm. This is the same interval through which Ca/Al, P/Al, and Fe/Al profiles increased as well (see the preceding). Sr/Al and Ba/Al, which at Site 794 showed a clear siliceous influence, record only an extremely slight increase through Unit II (Fig. 5B). Correlation coeffi-

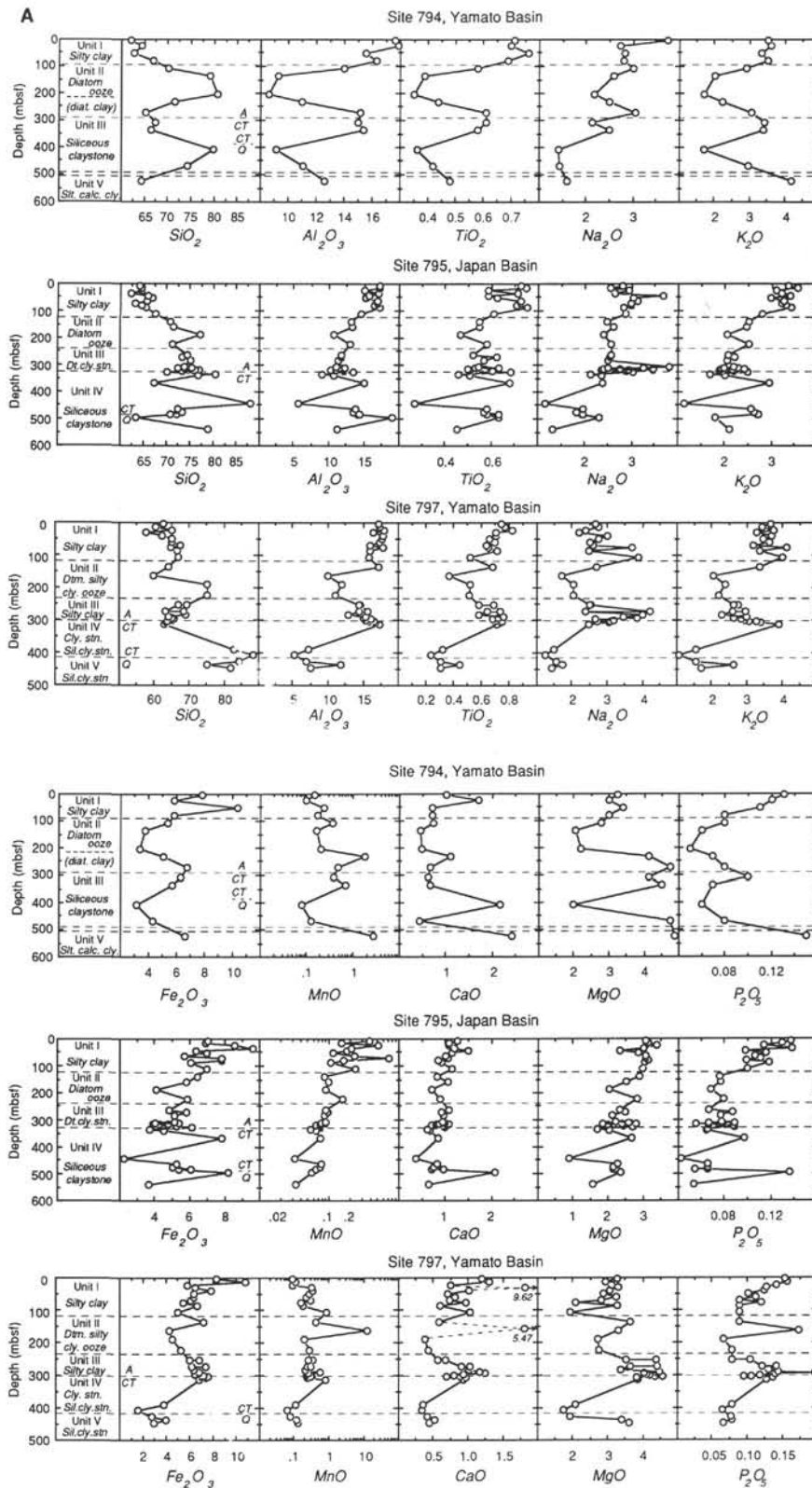


Figure 3. A. Downhole profiles of major element concentrations (wt%, volatile free) at Sites 794, 795, and 797. The siliceous component within the upper ~300 m is defined clearest at Site 794. Note the sporadic high concentrations of SiO_2 in Unit IV, Site 795. Isolated peaks of CaO, MgO, and P_2O_5 are most likely due to discrete manganese carbonates and stringers (cf. Matsumoto et al., this volume). See text for expanded lithologic descriptions. A, CT, and Q refer to opal-A, opal-CT, and quartz, respectively. Note the change in depth scale for Site 797. B. Al-normalized major element concentration profiles at Sites 794, 795, and 797. Symbols as in Figure 3A. The siliceous interval at Site 794 is clearly delineated by the Si/Al peak within Unit II. Note also the large Na/Al increase in Unit II at Site 794 and the greatly enriched Si/Al values in Unit V at Site 797. Note scale changes between sites.

B

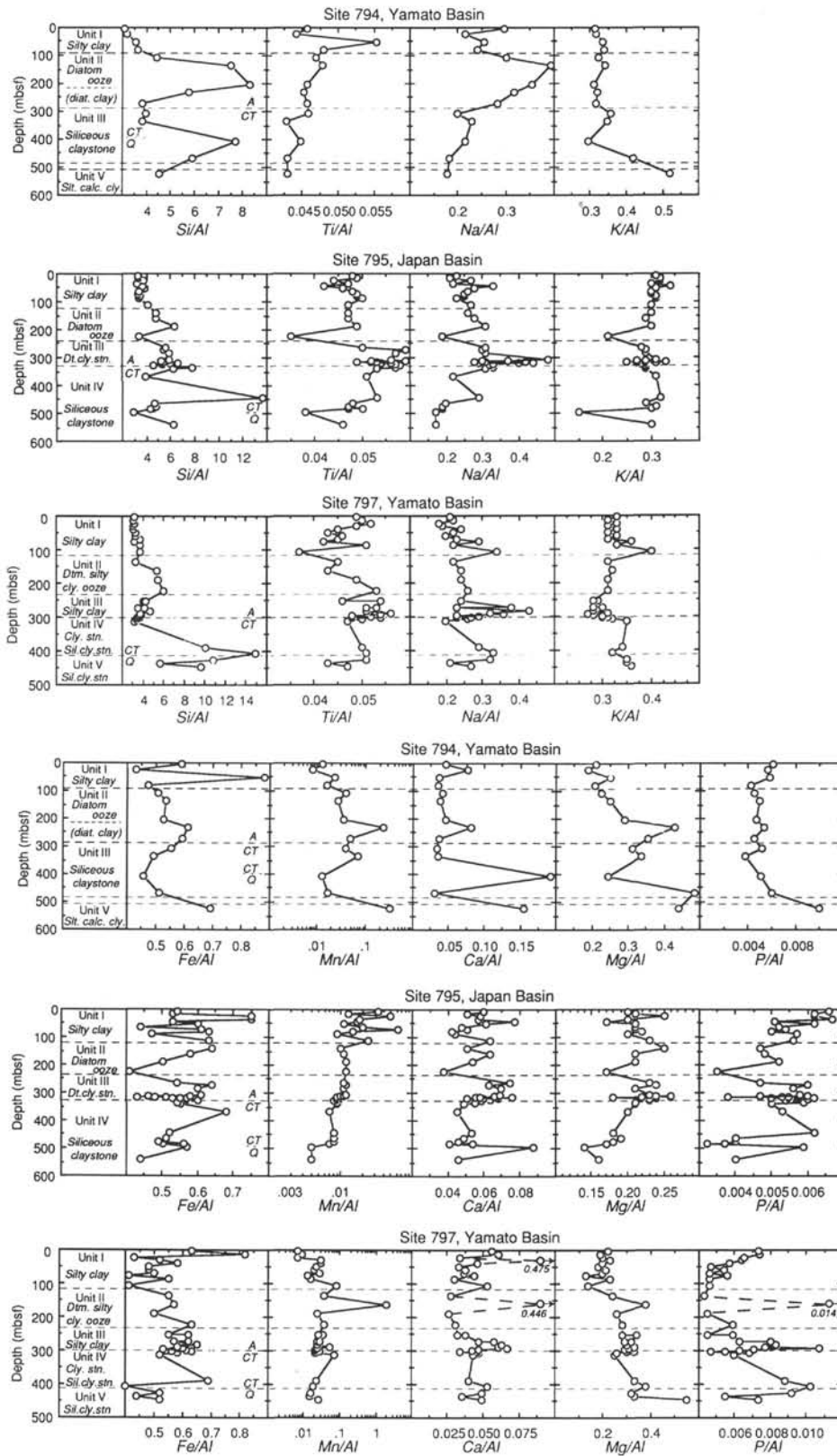


Figure 3 (continued).

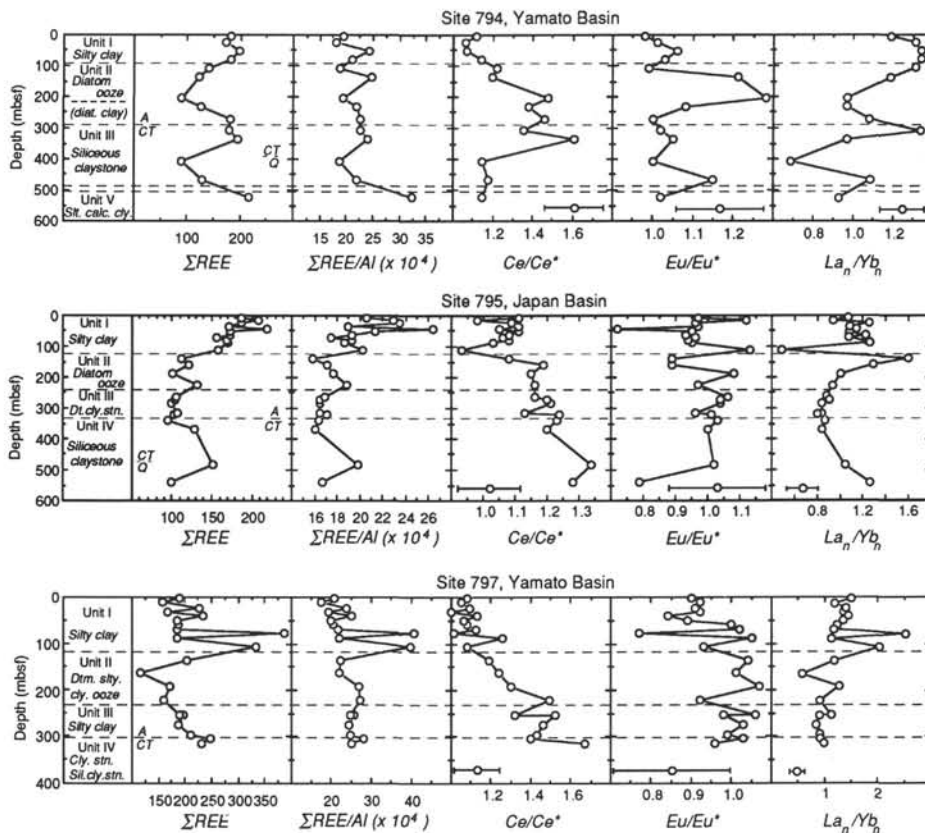


Figure 4. Downhole profiles of REE data at Sites 794, 795, and 797. Symbols as in Figure 3A. All Ce/Ce^* values increase essentially monotonically with depth, with the exception of depths >400 mbsf at Site 794 (see text). Note the large Eu/Eu^* increase at Site 794 through Unit II; this accompanies the Na/Al increase shown in Figure 3B. ΣREE enrichments in Unit I at Site 797 are due to the heavy-mineral component. Note the change in depth scale for Site 797. Error bars are of representative maximum error.

cient values suggest a moderate affiliation of Rb with aluminosilicates and of Sr with carbonates as well as aluminosilicates (Table 4).

Site 797

Major Elements

The SiO_2 profile at Site 797 is intermediate in nature to the SiO_2 profiles at Site 794 and Site 795, in that, like at Site 794, SiO_2 records some relative increase in concentration through the diatom ooze of Unit II (Fig. 3A). As at Site 795, however, the concentration increase at Site 797 is not clearly delineated. SiO_2 concentrations through Unit II reach a relative maximum only of ~75 wt% (dry). The lowest value within the diatomaceous interval ($SiO_2 = 59.8$ wt% at 163.9 mbsf) reflects dilution by Mn, Ca, and P, most likely caused by a manganese carbonate nodule or stringer in the particular sample (Fig. 3A). There is no discrete change in SiO_2 concentration across the opal-A/opal-CT diagenetic boundary. The high concentrations near the base of Unit IV and into Unit V reflect the increasing proportion of chert and porcellanite at depth. Other major element concentrations respond to the SiO_2 profile to varying degrees (Fig. 3B and Table 5). With the exception of the 163.9 mbsf data point (see the preceding), all of the major elements are diluted through the diatomaceous sediments of Unit II and appear to behave relatively similarly downhole. MgO increases with SiO_2 at depth, perhaps reflecting an association with the diagenetic SiO_2 phases.

The Si/Al profile at Site 797 delineates the siliceous intervals within Unit II as well as the pronounced diagenetic Si enrichment at

depth (Fig. 3B). Through Unit II, this Si/Al profile is similar to that at Site 794, although Si/Al ratios peak at ~6 at Site 797 and at ~8 at Site 794. Most other Al-normalized major element profiles do not present significant lithologic or diagenetic correlations. K/Al , however, seems to increase just below the opal-A/opal-CT transition and through Units IV and V, implying an affiliation with a diagenetically forming phase. Na/Al does not show the maximum within the diatomaceous interval that was observed at Site 794, although it does increase in the silty clay of Unit III (Fig. 3B). Ca/Al may also be higher in Unit III.

Rare Earth Elements

ΣREE increases slightly through the silty clays of Unit I (Fig. 4). The two high ΣREE (385 ppm at 78.3 mbsf; 334 ppm at 106.9 mbsf) each correspond with low Eu/Eu^* and high La_n/Yb_n , as well as with high Na_2O , K_2O , Y, Zr, and Nb, indicating a local heavy-mineral component specific to these samples (although not zircon, as La_n/Yb_n would be low), which does not occur at either Site 794 or Site 795. Although ΣREE may be slightly diluted through the uppermost diatomaceous sequences of Unit II, the lowest ΣREE at 163.9 mbsf reflects the influence of manganese carbonate, as mentioned previously. ΣREE increases continually from this relative minimum at 163.9 mbsf to maximum values of ~240 ppm just below the opal-A/opal-CT diagenetic transition. ΣREE is not responding to SiO_2 dilution ($r \sim 0$), and $r < 0.45$ between ΣREE and Al_2O_3 is the lowest implied aluminosilicate affiliation of all three sites (Table 6). These r values are markedly different from what is observed at either Site 794

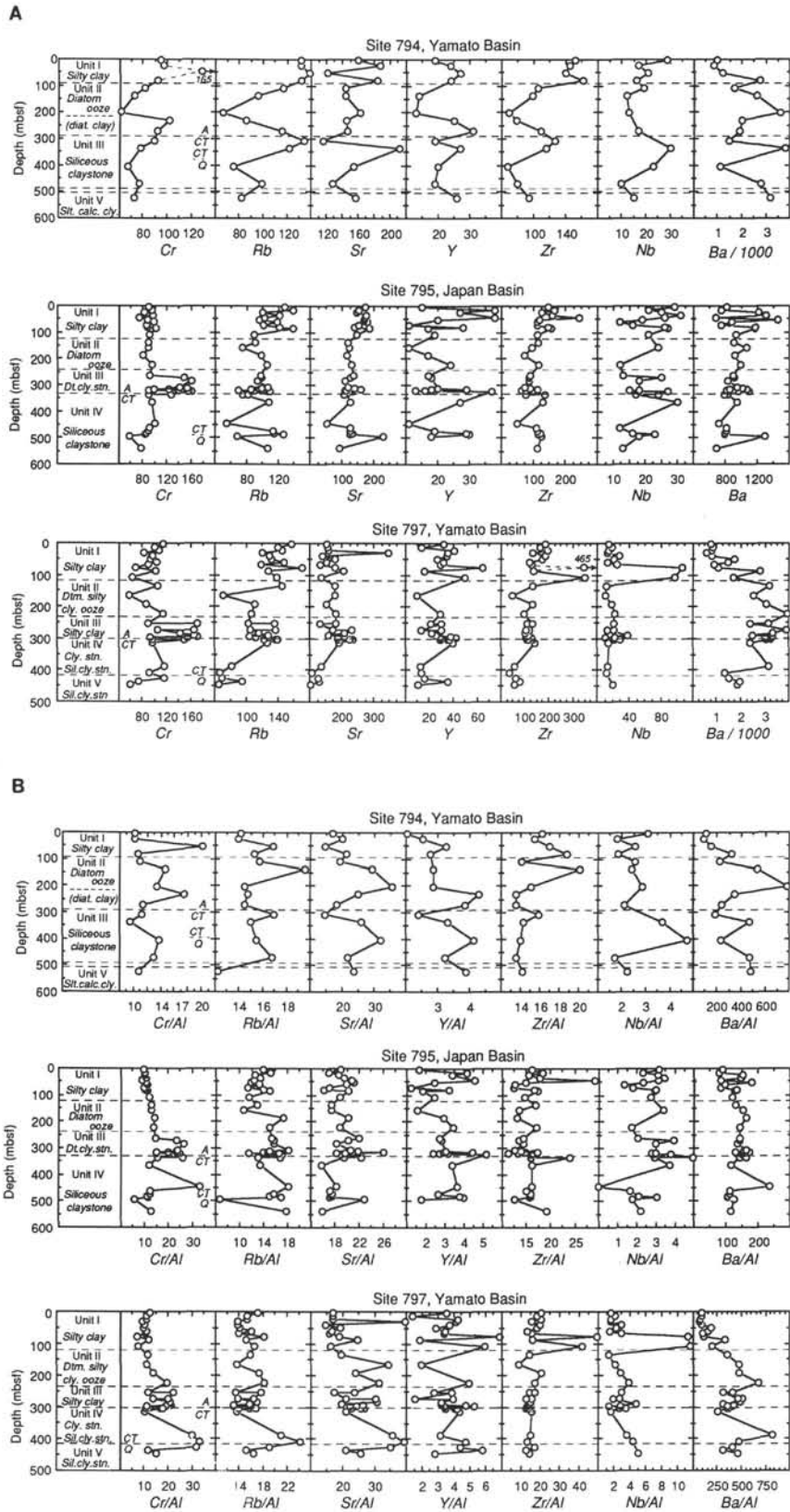


Figure 5. **A.** Downhole profiles of trace element concentrations (ppm) at Sites 794, 795, and 797. Symbols as in Figure 3A. Note the change in depth scale for Site 797. **B.** Al-normalized trace element concentration ($\times 10^4$) profiles at Sites 794, 795, and 797. Symbols as in Figure 3A. Note the change in depth scale for Site 797.

Table 3. Interelement comparison using correlation coefficient (*r*) values, Site 794.

	SiO ₂	Al ₂ O ₃	CaO	MgO	Na ₂ O	K ₂ O	Fe ₂ O ₃	MnO ^a	TiO ₂	P ₂ O ₅	Cr	Rb	Sr	Y	Zr	Nb	Ba
SiO ₂	1.00																
Al ₂ O ₃	-0.91	1.00															
CaO			1.00														
MgO	-0.55			1.00													
Na ₂ O	-0.52	0.65			1.00												
K ₂ O	-0.90	0.80		0.60		1.00											
Fe ₂ O ₃	-0.87	0.72			0.52	0.69	1.00										
^a MnO				0.58				1.00									
TiO ₂	-0.88	0.95			0.69	0.73	0.84		1.00								
P ₂ O ₅	-0.78	0.61	0.48			0.83	0.68		0.57	1.00							
Cr	-0.58	0.50					0.84		0.69		1.00						
Rb	-0.76	0.90			0.63	0.66	0.71		0.93			1.00					
Sr													1.00				
Y	-0.70	0.55		0.62		0.56	0.57	0.52	0.53					1.00			
Zr	-0.77	0.91			0.67	0.69	0.68		0.93	0.52					1.00		
Nb		0.49							0.45							1.00	
Ba									-0.46								1.00

Note: -*r* indicates negative correlation. -0.45 < *r* < 0.45 not shown (~95% confidence interval).

^a Determined without two nonrepresentative values from 232.5 and 523.7 mbsf (see text and Fig. 3).

Table 4. Interelement comparison using correlation coefficient (*r*) values, Site 795.

	SiO ₂	Al ₂ O ₃	CaO	MgO	Na ₂ O	K ₂ O	Fe ₂ O ₃	MnO	TiO ₂	P ₂ O ₅	Cr	Rb	Sr	Y	Zr	Nb	Ba
SiO ₂	1.00																
Al ₂ O ₃	-0.96	1.00															
CaO	-0.69	0.69	1.00														
MgO	-0.85	0.77		1.00													
Na ₂ O					1.00												
K ₂ O	-0.86	0.83		0.76		1.00											
Fe ₂ O ₃	-0.92	0.85	0.62	0.77		0.73	1.00										
MnO	-0.57	0.49		0.57		0.56	0.56	1.00									
TiO ₂	-0.89	0.88	0.49	0.84		0.81	0.77	0.45	1.00								
P ₂ O ₅	-0.87	0.82	0.71	0.71		0.69	0.83	0.53	0.77	1.00							
Cr											1.00						
Rb	-0.61	0.72		0.49		0.73			0.73	0.62		1.00					
Sr	-0.83	0.86	0.86	0.62	0.46	0.59	0.69		0.71	0.83		0.62	1.00				
Y						0.46						0.48		1.00			
Zr	-0.69	0.71	0.48	0.51		0.75	0.59		0.57	0.56	-0.47	0.46	0.58		1.00		
Nb							0.52			0.45						1.00	
Ba	-0.47			0.46			0.56			0.53			0.54				1.00

Note: -*r* indicates negative correlation. -0.45 < *r* < 0.45 not shown (~95% confidence interval). ΣREE vs. accumulation rate (g/cm²/k.y.) = -0.50.

Table 5. Interelement comparison using correlation coefficient (*r*) values, Site 797.

	SiO ₂	Al ₂ O ₃	CaO	MgO	Na ₂ O	K ₂ O	Fe ₂ O ₃	MnO	TiO ₂	P ₂ O ₅	Cr	Rb	Sr	Y	Zr	Nb	Ba
SiO ₂	1.00																
Al ₂ O ₃	-0.87	1.00															
CaO	-0.77	0.67	1.00														
MgO	-0.52			1.00													
Na ₂ O	-0.59	0.64	0.74		1.00												
K ₂ O	-0.78	0.94	0.60		0.57	1.00											
Fe ₂ O ₃	-0.81	0.82	0.74	0.53	0.59	0.68	1.00										
MnO						0.45		1.00									
TiO ₂	-0.83	0.93	0.70	0.58	0.64	0.80	0.88		1.00								
P ₂ O ₅	-0.73	0.66	0.89		0.53	0.57	0.73		0.76	1.00							
Cr				0.56	0.48						1.00						
Rb	-0.71	0.89	0.59		0.66	0.89	0.73		0.84	0.61		1.00					
Sr	-0.54	0.47		0.49	0.46		0.48		0.54				1.00				
Y		0.59			0.45	0.69			0.45			0.62		1.00			
Zr	-0.64	0.86			0.86	0.73			0.80	0.59		0.79		0.52	1.00		
Nb					0.56						0.57					1.00	
Ba											0.45		0.62				1.00

Note: -*r* indicates negative correlation. -0.45 < *r* < 0.45 not shown (~95% confidence interval). Determined without nonrepresentative values for MnO (163.9 mbsf), CaO (30.9, 163.9 mbsf), P₂O₅ (163.9, 294.4 mbsf), Zr-Nb (78.3, 163.9 mbsf), and Sr (30.9 mbsf) (see text and appropriate figures).

Table 6. Correlation coefficients (*r*) for REE data from Leg 127 squeeze-cake residues.

	Site 794				Site 795				Site 797			
	ΣREE	Ce/Ce*	Eu/Eu*	La _n /Yb _n	ΣREE	Ce/Ce*	Eu/Eu*	La _n /Yb _n	ΣREE	Ce/Ce*	Eu/Eu*	La _n /Yb _n
SiO ₂	-0.93		0.69	-0.49	-0.46	0.53		-0.68				
Al ₂ O ₃	0.79		-0.69	0.63	0.92	-0.62						
CaO			-0.46	-0.48	0.68	-0.52					-0.51	
MgO	0.61				0.83	-0.73			0.62			-0.73
Na ₂ O				0.58	0.53	-0.69		0.81				0.65
K ₂ O	0.93		-0.59	0.46	0.94	-0.65		0.55	-0.47	-0.47		0.62
Fe ₂ O ₃	0.80		-0.48	0.51	0.73	-0.48						
⁵⁵ MnO	0.48	0.81			0.52			0.70				
TiO ₂	0.76		-0.62	0.72	0.81	-0.49						
P ₂ O ₅	0.75	-0.52	-0.54		0.87	-0.66					-0.50	
Cr	0.47			0.51								-0.51
Rb	0.68		-0.54	0.81	0.70				-0.46			0.50
Sr					0.82	-0.63			0.46			-0.57
Y	0.68		-0.66					0.75				0.45
Zr	0.71		-0.49	0.76	0.71					-0.62		0.77
Nb			-0.57									
Ba		0.56	0.57						0.75	0.62		-0.60
ΣREE	1.00				1.00				1.00			
Ce/Ce*		1.00			-0.62	1.00				1.00		
Eu/Eu*	-0.57		1.00				1.00				1.00	
^b La _n /Yb _n				1.00			-0.69	1.00	0.53	-0.73		1.00

Note: -*r* indicates negative correlation. -0.45 < *r* < 0.45 not shown (-95% confidence interval). All data from Site 797 determined without nonrepresentative values for MnO (163.9 mbsf), CaO (30.9, 163.9 mbsf), P₂O₅ (163.9, 294.4 mbsf), ΣREE-Zr-Nb (78.3, 106.9 mbsf), Eu/Eu* (78.3 mbsf) La_n/Yb_n (78.3, 106.9, 163.9 mbsf) and Sr (30.9 mbsf) (see text and appropriate figures).

^a Determined for Site 794 without nonrepresentative values from 232.5 and 523.7 mbsf (see text).

^b Determined for Site 795 without nonrepresentative values from 110.2 mbsf (see text).

or Site 795, and suggest an influence on ΣREE of an additional sedimentary component other than the siliceous or aluminosilicate fraction. Note also that these *r* values are calculated while excluding the anomalously high ΣREE relating to high Y, Zr, and Nb near the base of Unit I. In general, ΣREE is correlated rather weakly at Site 797 compared with the other two sites; the only *r* > 0.8 is with Na₂O (*r* = 0.81), with other associations more weakly implied between MnO, K₂O, and Y (Table 6).

Ce/Ce* values average 1.09 ± 0.07 through the silty clay of Unit I, before increasing essentially monotonically to a maximum of 1.67 within Unit IV (Fig. 4). Eu/Eu* values average 0.90 ± 0.03 through the upper 49.8 m of Subunit IA, before increasing to slightly greater values (~1.01 ± 0.05) downhole to Subunit IVA. The low value (Eu/Eu* = 0.77) at 78.3 mbsf occurs in one of the samples with a potential heavy-mineral dominance (see the preceding). La_n/Yb_n decreases consistently downhole from near-surface values of ~1.4 to values within Unit IV ranging from ~0.9 to 1. The relatively high La_n/Yb_n = 2.53 (78.3 mbsf) and = 2.04 (106.9 mbsf) within Unit I is coincident with high ΣREE, Na/Al, Y/Al, and Zr/Al, as well as with low Eu/Eu*, as discussed previously. The low La_n/Yb_n = 0.57 at 163.9 mbsf corresponds with low ΣREE as well as with high MnO, CaO, and P₂O₅ and suggests REE fractionation into a manganese carbonate or phosphatic nodule or stringer.

Trace Elements

Trace element profiles at Site 797 in general show little variation through the silty clays of Unit I and the diatomaceous sequence of Unit II (Fig. 5A). The Y, Zr, and Nb peaks within Unit I are due to the heavy-mineral input discussed previously. Cr, Rb, and perhaps Sr increase into Unit III; as at Site 795, Cr is enriched greatly, yet shows no strong interelement correlation (Table 5). All elements, except for Nb, decrease in concentration below the opal-A/opal-CT transition through Unit IV. Al-normalized trace element profiles (Fig. 5B) indicate that most trace elements are affiliated with aluminosilicate phases, although some profiles (e.g., Sr/Al) increase at depth.

REEs IN JAPAN SEA SEDIMENTS

REE total concentrations and relative fractionations are potentially responding to the combined influences of (1) paleoceanographic and paleogeographic variation, (2) sediment lithology, and (3) diagenetic modification. The relative importance of each of these influences in controlling the REE composition of Japan Sea sediment at each site is synthesized in this section. Overall, the REEs are associated predominantly with the detrital fraction, which is diluted by biogenic input that is driven by productivity in the overlying water column. Due to the fact that the Japan Sea is an enclosed marginal basin dominated by terrigenous and biogenic sources, REE scavenging by metalliferous components is unimportant, although the process is a major influence elsewhere in marine sediment (e.g., Ruhlin and Owen, 1986; Murray et al., 1991).

Accordingly, paleogeographic position with respect to detrital and productivity inputs is the most important controlling influence on ΣREE concentrations within Japan Sea sediments (Fig. 6). Ce/Ce* does not respond to these inputs, as Ce/Ce* does not correlate with SiO₂ or Al₂O₃ to any significant degree, nor does the Ce/Ce* profile systematically change through diatomaceous intervals. ΣREE at both Sites 794 and 795 is controlled by terrigenous input from the nearby Japan Arc; the relatively high correlations of ΣREE with Al₂O₃ and K₂O suggest that most REEs are associated with clay minerals. Major element ratios (e.g., P₂O₅/Al₂O₃) are also similar to that of average shale. At Site 794, a pronounced Eu/Eu* increase through the diatomaceous Unit II may indicate an Eu-rich siliceous input or, alternatively, an additional feldspar contribution. In contrast to Sites 794 and 795, ΣREE at Site 797 correlates poorly with Al₂O₃ and the other major elements, and may be controlled locally and sporadically by a detrital heavy-mineral association. Such heavy minerals most likely would have originated from the rifted continental fragment composing the Yamato Rise, located nearby to the west (Fig. 1). Although there clearly is detrital input from the Yamato Rise beginning in the late Pliocene (Fig. 2), earlier inputs may be masked by diagenetic

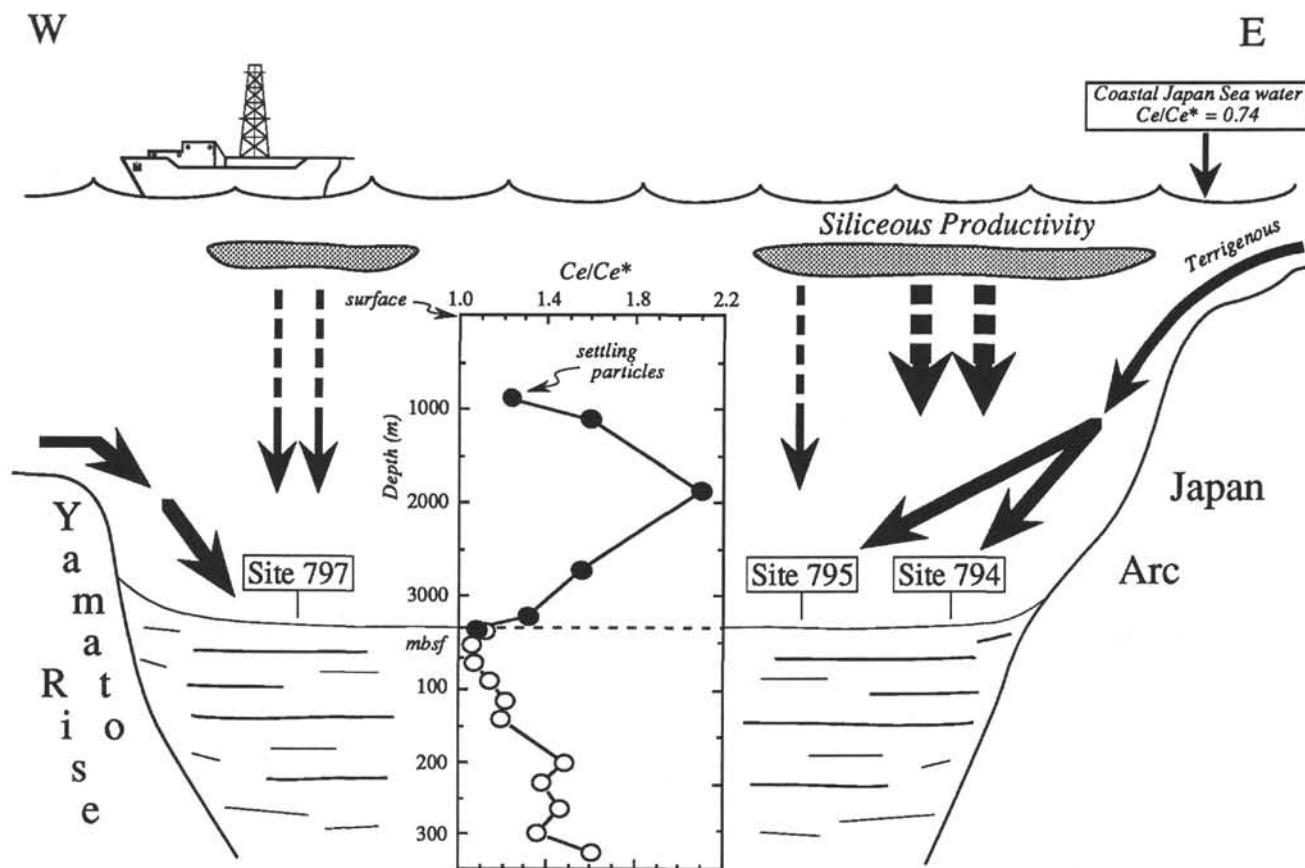


Figure 6. Schematic diagram summarizing processes that control Σ REE and Ce/Ce^* at Sites 794, 795, and 797. Sites are positioned according to their paleogeographic position relative to the detrital inputs from the Japan Arc and Yamato Rise as well as suggesting the relative significance of biogenic input from overlying water; sites are *not* positioned according to their actual location (Fig. 1). Note the change in scale between depth in seawater and sub-bottom depth. Coastal Japan Sea water data from Tanaka et al. (1990; Fig. 1), settling particle data from Masuzawa and Koyama (1989; Fig. 1), sediment data from this work (Site 794). Site 794 is heavily influenced by terrigenous input from the Japan Arc as well as by the biogenic component from the highly productive overlying water. Σ REE concentrations at Site 797 suggest input from the Yamato Rise. At Sites 795 and 797, the dashed line of productivity indicates the secondary role of siliceous input in controlling the Σ REE concentrations in the sediment. All three sites possess similar, diagenetically influenced, downhole Ce/Ce^* profiles; see the text for discussion of diagenetic mechanisms affecting the final preserved Ce/Ce^* of Japan Sea sediment.

alteration. There is little correlation between Σ REE and accumulation rate at any site (see discussion in Ruhlin and Owen, 1986; Murray et al., 1991), most likely because the accumulation rates are relatively similar and high throughout the Japan Sea (20–77 m/m.y.; Tamaki, Pisciotto, Allan, et al., 1990).

The detrital inputs (from the Japan Arc for Sites 794 and 795, from the Yamato Rise for Site 797) are diluted to varying degrees by the biogenic input from the overlying seawater. Σ REE values are most influenced by biogenic SiO_2 at Site 794, consistent with the location of Site 794 in the eastern portion of the Japan Sea, where upwelling and biogenic productivity were perhaps greatest. Σ REE values at Sites 795 and 797 also are diluted by the biogenic input, although not to the same extreme as Σ REE at Site 794. The two Yamato Basin sites reflect greater siliceous input than Site 795 in the Japan Basin.

REE abundances and relative fractionations within Japan Sea sediment do not record any basinwide paleoceanographic change. The consistent downhole increase in Ce/Ce^* at each site preserves diagenetic, not paleoceanographic, processes. Below ~400 mbsf at Site 794, Ce/Ce^* seems to decrease due to effects of SiO_2 diagenesis, as discussed previously. Although previous workers have related Ce/Ce^* values in sediments to the redox state of the overlying waters (e.g., Liu et al., 1988; see discussion of German and Elderfield, 1990a), there is no independent geologic, stratigraphic, paleontologic, or chemical data to suggest the existence of a monotonic and progressive oxygenation of

the Japan Sea which would be required to produce the Ce/Ce^* profile (Tamaki, Pisciotto, Allan, et al., 1990). In fact, as described earlier, bottom-water conditions ranged from oxic to dysaerobic throughout the Miocene, were in general well oxygenated during the late Miocene to Pliocene, and have recently included periods of anoxic deep water. None of these large-scale fluctuations in the oxygenation of bottom waters are recorded by Ce/Ce^* at any Leg 127 site. Indeed, because Ce reduction can occur under suboxic (not completely anoxic) conditions (e.g., German and Elderfield, 1990b), the independently documented variations of the Japan Sea dissolved oxygen should result in many oscillations of Ce/Ce^* values, were Ce/Ce^* in sediment responding faithfully to variations in the overlying water's oxygenation state. Furthermore, a comparison of downhole Ce/Ce^* profiles between Sites 794 and 797 (Fig. 7), which should record the same paleoceanographic signature because they are located within the same basin (Fig. 1), indicates that Ce/Ce^* correlates slightly better with depth than with age.

The consistent downhole increase of Ce/Ce^* instead is explained best by diagenetic fractionations. Masuzawa and Koyama (1989) measured large positive Ce anomalies (-1.56 ± 0.34) for settling particles of undifferentiated composition in the Japan Sea and concluded that Ce is preferentially removed from Japan Sea waters, in association with Mn. This Ce is most likely Ce(IV), because Ce(III) behaves similarly to the other trivalent REEs. Based on the less extreme positive Ce anomalies

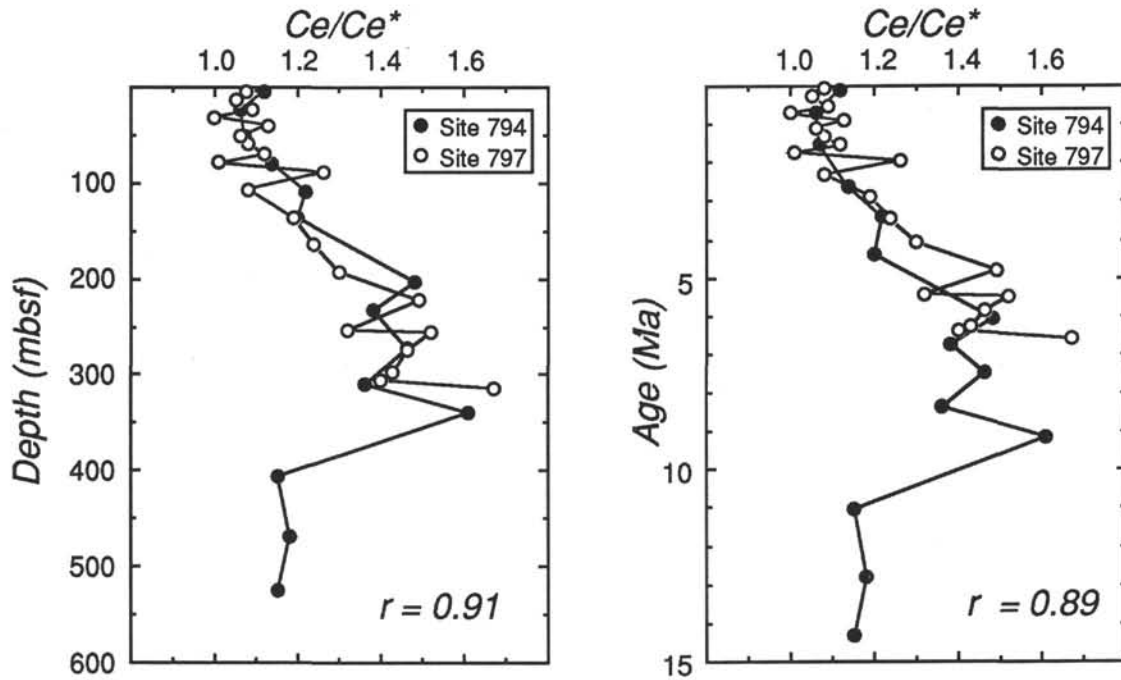


Figure 7. Profiles of Ce/Ce^* at Sites 794 and 797 plotted downhole vs. depth and age. Note the overlapping plots of the two sites and the slightly higher correlation coefficient when plotted vs. depth; better correlations would be expected vs. age, not depth, were Ce/Ce^* responding to paleoceanographic variations in the overlying water.

from the surface sediment ($Ce/Ce^* = 1.07$) than in the settling particles, Masuzawa and Koyama (1989) further suggested that the Ce-bearing Mn(IV) oxide phases are liberated in conjunction with the decomposition of organic material at or near the seafloor. By monitoring both the bulk flux and Al flux near the seafloor they were able to rule out significant resuspension of bottom sediment in their particulate samples (Masuzawa and Koyama, 1989). We note further that much of the Ce liberation must be occurring while particles are relatively high in the water column, as shown by the substantial decrease in particulate Ce/Ce^* below 1870-m water depth (Fig. 6). The fact that Ce is cycling actively in the water column suggests that Ce may also be relatively labile during diagenetic reactions within the sediment. Indeed, by definition, the increasing Ce/Ce^* profile through at least the upper 350 m of each site indicates that with continued burial Ce concentrations are increasing in the sediment, relative to concentrations of the neighboring trivalent LREEs. Whether this relative Ce increase is due to transfer of Ce from interstitial waters to sediment or to removal of other LREEs from sediment remains to be seen; examination of the La_n/Yb_n ratio may help differentiate between the two processes. The following two paragraphs address this topic.

La_n/Yb_n values are mostly within the range of postulated average terrigenous input (~1.0–1.3; Sholkovitz, 1990; Condie, 1991), excluding the obvious nonrepresentative values discussed previously. Other subtle yet systematic deviations from this average are apparent at all three sites and, with the notable exception of Unit IV at Site 795, La_n/Yb_n tends to increase with depth. These trends potentially reflect one or more of the following testable hypotheses: (1) variation in REE fractionation during adsorption from seawater, (2) changes in REE input associated with changes in sediment sources to the basin, or (3) diagenetic remobilization and exchange with interstitial water. Mechanism (1) is improbable, because REE fractionation from seawater would preferentially remove LREEs from seawater and add them to sediment, thereby increasing—not decreasing—sedimentary La_n/Yb_n values. Mechanism (2) may explain some of the variation, although its impact is unlikely to be large, given the relative uniformity of mixed terrestrial sediments like these of similar age and tectonic

environment (e.g., Taylor and McLennan, 1985) and that there are only slight differences in post middle Miocene clay mineralogy throughout these sites, as discussed previously (Fagel et al., 1991). La_n/Yb_n values may, however, tend to decrease through the diatomaceous sequences, which may reflect primary compositional or adsorptive differences between biogenic and terrigenous particles. Mechanism (3) would require either the successive loss of LREEs from sediment to interstitial water, which seemingly contradicts the Ce/Ce^* increase discussed previously, or the transfer of HREEs from sediment to interstitial water, which also is improbable, given the relatively restricted behavior of HREEs in other diagenetic and marine environments (e.g., Fleet, 1984; Sholkovitz et al., 1989). If diagenetic remobilization of LREEs actually is occurring, however, transfer of LREEs from sediment to interstitial water must be occurring to LREEs with the exception of Ce, as Ce/Ce^* increases with depth. This would require Ce, behaving anomalously due to its higher oxidation state, to be retained on the sediment while the remaining LREEs are transferred to interstitial waters.

Although Ce/Ce^* does not correlate well with La_n/Yb_n for all points at a given site (with the exception of Site 797; Table 5), there nevertheless may be a genetic relationship between the loss of LREEs (except for Ce) from sediment and development of a positive Ce anomaly. It is necessary to evaluate whether the hypothesized LREE transfer from sediment to the interstitial water could cause or accentuate the downhole Ce/Ce^* increase observed at all sites. Considering first Site 797 because the La_n/Yb_n and Ce/Ce^* profiles are nearly linear through the entire sequence and it is the only site with a suggested correlation between La_n/Yb_n and Ce/Ce^* (Table 6), the consistent decrease from near-surface La_n/Yb_n values of ~1.40 to La_n/Yb_n ~ 0.95 at depth requires a 32% loss of La, with respect to Yb. Ce* would also decrease by 32%, resulting in an overall ~50% increase in the calculated Ce/Ce^* . At Site 797, then, if all Ce is retained on sediment, loss of LREEs with depth would predict a Ce/Ce^* change from ~1.1 to ~1.7. This predicted value agrees well with the observed profile at Site 797, where Ce/Ce^* reaches maximum values of ~1.67 at depth. The data therefore are consistent with

sympathetic generation of a positive Ce anomaly due to LREE transfer from sediment to interstitial water, with Ce(IV) retained by the sediment. At Site 794 (0–300 mbsf, over which Ce/Ce* increases smoothly), the predicted Ce/Ce* due to LREE loss is ~1.4, again agreeing well with the observed Ce/Ce* of ~1.4. At Site 795 (using La_n/Yb_n through Unit II and Unit III because Ce/Ce* is relatively constant within Unit I), the calculations predict an ~70% increase in Ce/Ce*, more than enough to account for the observed Ce/Ce* change of ~20% through the same interval. The increasing La_n/Yb_n through Unit I, however, is not paralleled by a Ce/Ce* change, nor is the increasing La_n/Yb_n through Unit IV, indicating that at Site 795 there may not be a causal link between LREE behavior and downhole development of the positive Ce anomaly, and that other processes seem to be masking LREE behavior. Considering all sites, then, at Sites 794 and 797 (both in the Yamato Basin) there may be a genetic relationship between LREE loss and generation of a positive Ce anomaly, whereas at Site 795 (Japan Basin) the exact relationship between LREE behavior and Ce/Ce* remains unclear. This may reflect fundamental contrasts between sedimentation in the two basins (Fig. 1), with the Yamato Basin sediments in general recording a greater influence by biogenic input. Overall, the evidence strongly suggests that the consistent downhole increase in Ce/Ce* may be a passive response to LREE loss and need not involve significant remobilization of Ce. The contrast between the LREE transfer from sediment to interstitial water in the Japan Sea and the previous observations documenting LREE uptake by sediment from interstitial water in estuaries (e.g., Sholkovitz et al., 1989) probably reflects the major differences between the deep Japan Sea environment and the shallow estuarine systems; these contrasts include, but are not limited to, sedimentation rate, age of burial and duration of diagenetic reactions recorded by sediment/interstitial water, depth of profile, and organic matter content. Note also that the diagenetic processes documented in the recent and shallowly buried estuaries (Sholkovitz et al., 1989) are not necessarily incompatible with the fractionations documented in the Japan Sea deeply buried and deep-water sediment. For example, transfer of LREE to sediment may be occurring in the uppermost 40 cm of the Japan Sea sediment, as observed in the estuaries; we would not, however, be able to observe these shallow fractionations as our data profiles begin at 3 mbsf.

We further test the hypothesis of LREE (except Ce) transfer from sediment to interstitial water and assess the budget of Ce in the Japan Sea by combining the water column Ce/Ce* profile of Masuzawa and Koyama (1989), located 50–100 km north of Site 794 (Fig. 1), and the downhole Ce/Ce* profile to ~300 mbsf at Site 794 (Fig. 6). In order to track the behavior of Ce with respect to its neighboring LREEs and average shale, in addition to Ce/Ce* we use the calculated $Ce_{excess} = Ce_{ex} = Ce_{sample} - [La_{sample} \times (Ce_{shale}/La_{shale})]$, which facilitates comparison of percent concentration change in Ce with respect to La, in units of ppm, and is also a more precise measurement than Ce/Ce*. A large exchange of Ce, with respect to the other LREEs, occurs within the water column, as nearly 20% of the Ce_{ex} composing the large positive Ce anomaly on settling particles is recycled during descent through the water column (Ce_{ex} decreases from 16.3 to ~13 ppm, with Ce/Ce* decreasing from ~2.10 to ~1.28; Masuzawa and Koyama, 1989). Coastal waters from the southeastern Japan Sea average Ce/Ce* ~0.74 (Tanaka et al., 1990); although these coastal waters are distant from the Site 794 region (Fig. 1), this relative Ce depletion in water balances the smallest observed enrichment of ~1.28 in the settling particles (based on an initial Ce/Ce* ~1.00). Therefore, in addition to the 20% Ce_{ex} recycled in the water column, there may be a further 13-ppm Ce_{ex} that survives water column recycling and is transported to the seafloor environment. This 13 ppm represents the maximum amount of Ce, contributed by the particles, that is recycled at or near the seafloor (Fig. 6; Masuzawa and Koyama, 1989). The surficial sediment Ce_{ex} of ~8 ppm (Ce/Ce* ~1.07) indicates that 38% of this maximum Ce_{ex} is released to seawater at the seafloor. Thus, because of the great Ce exchange occurring at the sediment/water

interface, there is not a significant source of Ce_{ex} to the deeply buried sediment. For example, if at Site 794 the entire Ce_{ex} of 8 ppm remaining in the surface sediment (~10% Ce_{total}) was released to shallow pore waters and subsequently transferred back to the sediment upon deeper burial, it would generate a positive Ce anomaly of only Ce/Ce* ~1.1, far less than the observed Ce/Ce* of ~1.5. Therefore, the increases in Ce/Ce* with depth are not due to remobilized Ce from the original input(s). While it is difficult to refine further potential diagenetic mechanisms without deeply buried REE interstitial-water data, the data sets and the Ce budget strongly suggest that the downhole increase in sediment Ce/Ce* is a passive response to the behavior of the other LREEs and predict the successive downhole addition of LREEs to deeply buried interstitial waters.

SUMMARY AND CONCLUSIONS

The most important variation in sedimentary chemical composition throughout the Japan Sea is the increase in SiO₂ concentration through Pliocene diatomaceous sequences, which dilutes most of the other major and trace element components by various degrees. This biogenic input is largest at Site 794 (Yamato Basin), moderately developed at Site 797 (Yamato Basin), and of only minor importance at Site 795 (Japan Basin) and potentially reflects basinal contrasts in productivity, with the Yamato Basin in general recording greater biogenic input than the Japan Basin and the easternmost sequence of Site 794 lying beneath the most productive waters of all three sites. There are few large or systematic changes in solid-phase chemistry resulting from the opal-A/opal-CT or opal-CT/quartz silica phase transformations. With the exception of certain elements on a site-specific basis, most major and trace element concentrations are controlled by the aluminosilicate fraction of the sediment. The increasing amount of diagenetic phases with depth commonly results in greater concentrations of SiO₂, CaO, and MnO, due to their respective affiliation(s) with diagenetic silica phases and manganese carbonate nodules and stringers.

ΣREE concentrations in the Japan Sea are strongly dependent upon the paleoceanographic position of a given site with respect to terrigenous and biogenic sources. ΣREE values at Site 794 are strongly diluted by the biogenic component through Unit II and Unit III, and in general correspond well to aluminosilicate chemical indices. Eu/Eu* values at Site 794 reach a maximum through the diatomaceous sequence as well, which most likely reflects a relative Eu enrichment of the siliceous component or may suggest the slight incorporation of a detrital feldspar phase. ΣREE at Site 795 also is strongly affiliated with aluminosilicate phases yet is diluted only slightly by siliceous input. At Site 797, also in the Yamato Basin, ΣREE does not correspond well with aluminosilicate indices, is correlated moderately to siliceous input, and appears sporadically and locally influenced by detrital heavy minerals from the nearby rifted continental fragment composing the Yamato Rise.

Ce/Ce* profiles at all three sites increase essentially monotonically with depth (except below 400 mbsf at Site 794) and record progressive diagenetic LREE relative fractionation. The observed Ce/Ce* increases are not responding to changes in the paleoceanographic oxygenation state of the overlying water, as there are no independent geologic, stratigraphic, paleontologic, or additional chemical data to suggest the existence of a monotonic and progressive oxygenation of the Japan Sea. Ce/Ce* correlates better with depth than with age at the two Yamato Basin sites.

Preliminary calculations suggest that at Sites 794 and 797 the transfer of LREEs (with the exception of Ce) from sediment to interstitial water may account for all of the observed relative Ce increase. Therefore, the observed downhole increase in Ce/Ce* may be a passive response to diagenetic behavior of the non-Ce LREEs. At Site 795, the overall lack of correlation between Ce/Ce* and La_n/Yb_n suggests that other processes are occurring which mask the diagenetic behavior of all LREEs. First-order calculations of the relative Ce budget suggest that ~20% of the Ce_{excess} adsorbed by

settling particles is recycled within the water column and that an additional ~38% is recycled at or near the sediment/water interface (data from Masuzawa and Koyama, 1989). Thus, because the remaining 45% Ce_{ex} translates to 8-ppm Ce_{ex} and equals only ~10% Ce_{total} , there is not a significant source of Ce to the deeply buried sediment, further suggesting that the downhole increase in Ce/Ce^* is a passive response to behavior of the other LREEs. The REE chemistry of the Japan Sea sediment therefore predicts the successive downhole addition of LREEs to interstitial waters with deep burial.

ACKNOWLEDGMENTS

We thank Dr. E. H. De Carlo and an anonymous reviewer for their comments and Dr. D. Nobes (U. of Waterloo, Canada) for providing the physical-property residue samples. We thank the most helpful and professional technical staff of the ODP, and particularly the Leg 127 shipboard personnel of MaryAnn Cusimano and Luis Alvarez (chemistry technicians), Matt Mefferd (assistant lab officer), Barry Weber (electronic technician), and Don Sims (marine technician, X-ray lab). Larry Bernstein and Burney Hamlin assisted in keeping the shipboard chemistry lab running smoothly. We also thank the Leg 127 co-chief scientists (Drs. K. Pisciotto and K. Tamaki) and ODP staff scientist (Dr. J. A. Allan) and curatorial representative (Peggy Myre Murray) for accommodating last-minute sample requests and for providing essential shipboard support. Additionally, we thank G. Hunt and J. Bazan at LLNL for assistance with the ICP-MS, as well as G. Anderson and G. Phelps for the sample preparation at University of California at Berkeley. This work was partially supported by the Institute for Geophysics and Planetary Physics at Lawrence Livermore National Laboratory Grant # 90-41 and performed under the auspices of the U.S. Department of Energy by Lawrence Livermore National Laboratory under Contract W-7405-Eng-48. The work was performed while R. W. Murray held a shore-based JOI/USSAC Ocean Drilling Fellowship, and funded additionally by a JOI/USSAC Cruise Science Support grant to R. W. Murray.

This manuscript contains material that is excerpted for a shorter manuscript, emphasizing REE behavior, published by *Geochimica et Cosmochimica Acta*. Both manuscripts were submitted simultaneously in accordance with ODP policy regarding dual submittal of ODP results, and with full knowledge of the executive editor of *Geochimica*. We thank R. L. Cullers, C. R. German, R. L. Korotev, and R. A. Schmitt for their reviews of the *Geochimica* paper, many of which were incorporated in this longer ODP contribution.

REFERENCES

Boles, J. R., and Franks, S. G., 1979. Clay diagenesis in Wilcox Sandstones of southwest Texas: implications of smectite diagenesis on sandstone cementation. *J. Sediment. Petrol.*, 49:55-70.
 Condie, K. C., 1991. Another look at rare earth elements in shales. *Geochim. Cosmochim. Acta*, 55:2527-2531.
 Donnelly, T. W., and Merrill, L., 1977. The scavenging of magnesium and other chemical species by biogenic opal in deep-sea sediments. *Chem. Geol.*, 19:167-186.
 Dymek, R. F., and Gromet, L. P., 1984. Nature and origin of orthopyroxene megacrysts from the St.-Urbain anorthosite massif, Quebec. *Can. Mineral.*, 22:297-326.

Elderfield, H., 1988. The oceanic chemistry of the rare-earth elements. *Philos. Trans. R. Soc. London A*, 325:105-126.
 Fagel, N., Andre, L., Chamley, H., Debrabant, P., and Jolivet, L., 1991. Clay sedimentation in a back-arc environment: the Japan Sea, ODP Leg 127. *Terra*, 3:283. (Abstract)
 Fleet, A. J., 1984. Aqueous and sedimentary geochemistry of the rare earth elements. In Henderson, P. (Ed.), *Rare Earth Element Geochemistry*: New York (Elsevier), 343-373.
 German, C. R., and Elderfield, H., 1990a. Application of the Ce anomaly as a paleoredox indicator: the ground rules. *Paleoceanography*, 5:823-833.
 ———, 1990b. Rare earth elements in the NW Indian Ocean. *Geochim. Cosmochim. Acta*, 54:1929-1940.
 Gromet, L. P., Dymek, R. F., Haskin, L. A., and Korotev, R. L., 1984. The "North American Shale Composite": its compilation, major and trace element characteristics. *Geochim. Cosmochim. Acta*, 48:2469-2482.
 Haskin, M. A., and Haskin, L. A., 1966. Rare earths in European shales, a re-determination. *Science*, 154:507-509.
 Hower, J., Eslinger, E. V., Hower, M. E., and Perry, E. A., 1976. Mechanism of burial metamorphism of argillaceous sediment: 1. Mineralogical and chemical evidence. *Geol. Soc. Am. Bull.*, 87:725-737.
 Jarvis, I., and Jarvis, K. E., 1985. Rare-earth element geochemistry of standard sediments: a study using inductively coupled plasma spectrometry. *Chem. Geol.*, 53:335-344.
 Liu, Y.-G., Miah, M.R.U., and Schmitt, R. A., 1988. Cerium: a chemical tracer for paleo-oceanic redox conditions. *Geochim. Cosmochim. Acta*, 52:1361-1371.
 Masuzawa, T., and Koyama, M., 1989. Settling particles with positive Ce anomalies from the Japan Sea. *Geophys. Res. Lett.*, 16:503-506.
 McLennan, S. M., 1989. Rare earth elements in sedimentary rocks: influence of provenance and sedimentary processes. In Lipin, B. R., and McKay, G. A. (Eds.), *Geochemistry and Mineralogy of the Rare Earth Elements*. Rev. Mineral., 21:169-200.
 Murray, R. W., Buchholtz ten Brink, M. R., Gerlach, D. C., Russ, G. P., III, and Jones, D. L., 1991. Rare earth, major and trace elements in chert from the Franciscan Complex and Monterey Group, California: assessing REE sources to fine-grained marine sediments. *Geochim. Cosmochim. Acta*, 55:1875-1895.
 Ruhlin, D. E., and Owen, R. M., 1986. The rare earth element geochemistry of hydrothermal sediments from the East Pacific Rise: examination of a seawater scavenging mechanism. *Geochim. Cosmochim. Acta*, 50:393-400.
 Sholkovitz, E. R., 1988. Rare earth elements in the sediments of the North Atlantic Ocean, Amazon Delta, and East China Sea: reinterpretation of terrigenous input patterns to the oceans. *Am. J. Science*, 288:236-281.
 ———, 1990. Rare earth elements in marine sediments and geochemical standards. *Chem. Geol.*, 88:333-347.
 Sholkovitz, E. R., Piepgras, D. J., and Jacobsen, S. B., 1989. The pore-water chemistry of rare earth elements in Buzzards Bay sediments. *Geochim. Cosmochim. Acta*, 53:2847-2856.
 Tamaki, K., Pisciotto, K., Allan, J., et al., 1990. *Proc. ODP, Init. Repts.*, 127: College Station, TX (Ocean Drilling Program).
 Tanaka, M., Shimizu, H., and Masuda, A., 1990. Features of the heavy rare-earth elements in seawater. *Geochem. J.*, 24:39-46.
 Taylor, S. R., and McLennan, S. M., 1985. *The Continental Crust: Its Composition and Evolution*: Oxford (Blackwell Scientific).

Date of initial receipt: 18 March 1991

Date of acceptance: 29 August 1991

Ms 127/128B-176